Controlled Access to Mixed-Metal Pyridazine-Linked Cryptates

Tanya K. Ronson,[a] Jane Nelson,[b,c] Geoffrey B. Jameson,[d] John C. Jeffery,[e] and Sally Brooker*[a]

Keywords: Cryptates / Cyclic voltammetry / Heterometallic complexes / N ligands / Structure elucidation

The pyridazine-linked cryptand L [formed by the 3+2 condensation of 3,6-diformylpyridazine with tris(2-aminoethyl)amine (tren)] has been used to generate a series of heterodinuclear cryptates by a one-pot two-step method. The cryptates $[Mn^{II}Cu^{I}L](ClO_4)_2(BF_4)$, $[Fe^{II}Cu^{I}L](BF_4)_3{\cdot}CH_3CN$ and $[Ni^{II}Cu^{I}L](BF_4)_3{\cdot}H_2O$ have been structurally characterized, with elemental analyses and mass spectroscopic data providing further evidence of their heterodinuclear nature. The synthesis, structures and characterisation of the corresponding mononuclear cryptates $[M^{II}L](X)_2$ (M = Mn, Fe, Ni, X = BF_4^- or ClO_4^-) are also reported, along with the synthesis and characterisation of the homodinuclear dizinc(II) and disodium(I) cryptates, $[Zn_2L](ClO_4)_4$ and $[Na_2L](CF_3SO_3)_2$. Electrochemical studies on the heterodinuclear cryptates in CH_3CN indicate that the presence of the divalent cation influences the electrochemical potential and reversibility of the $Cu^{I} \rightarrow Cu^{II}$ oxidation with the redox potential of the Cu^{I}/Cu^{II} couple being inversely correlated with the distance between the two metal ions in the solid state as determined by X-ray crystallography. The previously synthesised $[Co^{II}Cu^{I}L](BF_4)_3$ is an exception to this trend, probably due to oxidation of the Co^{II} ion prior to that of the Cu^{I} ion.

Introduction

There are now a large number of cryptates reported and these have recently been reviewed.[1] However, very few mixed-metal cryptates have been prepared. Such heterodinuclear complexes are of interest as models for metalloenzyme active sites[2] and to study the mutual influences of the two metal centres on the electronic, magnetic and electrochemical properties of these systems.[3] Heterodinuclear cryptates synthesised to date include several structurally characterised transition metal-lanthanide cryptates of iminophenolate cryptands[4] and a $Fe^{II}Co^{II}$ cryptate of another iminophenolate cryptand,[5] although in this case the structural data are ambiguous.[6] An imidazolate-bridged $Zn^{II}Cu^{II}$ cryptate of an octa-amino cryptand has also been reported and is of interest as a model compound for the CuZn family of superoxide dismutases.[7]

Recently, we developed a system where we were able to isolate the mixed-valent complex $[Cu^{II}Cu^{I}L](BF_4)_3$ and the heterodinuclear complex $[Co^{II}Cu^{I}L](BF_4)_3$ [L is the cryptand formed by the 2+3 condensation of 3,6-diformylpyridazine with tris(2-aminoethyl)amine (tren), Figure 1].[8] In addition, we prepared the mononuclear cryptates $[Cu^{II}L](BF_4)_2$ and $[Co^{II}L](BF_4)_2$ of the same symmetrical cryptand.[9,10] This is possible because the binding of a single stereochemically demanding cation alters the conformation of the host in such a way as to prevent the formation of a homodinuclear complex. The resulting unsymmetrical mononuclear cryptates still have up to eight donor atoms available for coordination and so are able to bind a second non-stereochemically demanding cation such as copper(I)

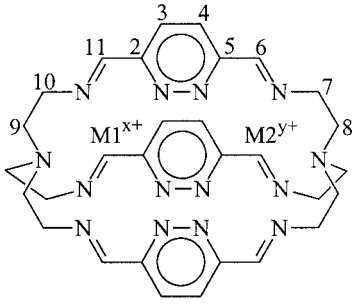

Figure 1. Schematic representation of the complex cations of the pyridazine containing cryptand L which have been prepared in this study, numbered as used in the NMR spectroscopic data assignments; note: M2^{y+} is (a) the same as M1^{x+} in the homodimetallic complexes, (b) absent in the monometallic complexes, (c) the Cu^{I} ion in the heterobimetallic complexes

[a] Department of Chemistry, University of Otago,
P. O. Box 56, Dunedin, New Zealand
Fax: (internat.) +64-3-479-7906
E-mail: sbrooker@alkali.otago.ac.nz
[b] School of Chemistry, Queens University of Belfast,
Belfast BT9 5AG, Northern Ireland
[c] Biomedical Sciences, University of Ulster,
Coleraine BT52 1SA, Northern Ireland
[d] Institute of Fundamental Sciences − Chemistry, Massey University,
P. O. Box 11222, Palmerston North, New Zealand
[e] School of Chemistry, University of Bristol,
Cantock's Close, Bristol BS8 ITS, United Kingdom
Supporting information for this article is available on the WWW under http://www.eurjic.org or from the author.

  DOI: 10.1002/ejic.200400068

using four of these donor atoms, resulting in heterodinuclear complexes. Mixed metal complexes of symmetrical ligands are very unusual for acyclic systems and there are only a few examples for macrocyclic ligands.[4,5,7,11]

In this paper we report on the synthesis and characterisation of the heterodinuclear cryptates $[Mn^{II}Cu^{I}L](ClO_4)_2(BF_4)$, $[Fe^{II}Cu^{I}L](BF_4)_3{\cdot}CH_3CN$ and $[Ni^{II}Cu^{I}L](BF_4)_3{\cdot}H_2O$. We have completed a systematic study of the effect of the divalent cation on the copper(I) ion across the series $[M^{II}Cu^{I}L](X)_3$ (M = Mn, Fe, Co, Ni, Cu; X = BF_4^- or ClO_4^-), focussing on the electrochemical properties of these systems. In this context, it is useful to have a complex of a non-redox active cation; hence we have prepared $[Zn_2L](ClO_4)_4$. For completeness, the mononuclear cryptates $[Mn^{II}L](ClO_4)_2$, $[Fe^{II}L](BF_4)_2$ and $[Ni^{II}L](X)_2$ (X = BF_4^-, ClO_4^-) are also reported.

Results and Discussion

Synthesis and Characterisation of Mononuclear and Homodinuclear Cryptates

As we had previously observed that L readily forms the mononuclear cryptates $[Co^{II}L](BF_4)_2$ and $[Cu^{II}L](BF_4)_2$,[9,10] attempts were made to synthesise other mononuclear cryptates of first-row transition metals. The cryptates $[Mn^{II}L](ClO_4)_2$ and $[Ni^{II}L](X)_2$ (X = BF_4^-, ClO_4^-) were readily obtained in good purity and yield from the addition of one equivalent of the appropriate metal salt to L. The synthesis of $[Fe^{II}L](BF_4)_2$ proceeded in a lower yield and was sensitive to air and traces of solvent water.

Infrared spectra of the mononuclear cryptates confirmed that the L cryptand remains intact {imine at 1652 cm^{-1} for $[Mn^{II}L](ClO_4)_2$, 1638 cm^{-1} for $[Fe^{II}L](BF_4)_2$ and 1647 cm^{-1} for $[Ni^{II}L]^{2+}$} and confirms the presence of the expected anions {1116 and 1088 cm^{-1} for $[Mn^{II}L](ClO_4)_2$, 1052 and 1032 cm^{-1} for $[Fe^{II}L](BF_4)_2$, 1050 cm^{-1} for $[Ni^{II}L](BF_4)_2$ and 1083 cm^{-1} for $[Ni^{II}L](ClO_4)_2$}. In each case, the microanalyses support the proposed formula. The electrospray mass spectra show peaks for the successive loss of the two counterions. The molar conductivity values of 280 $mol^{-1}\,cm^2\,\Omega^{-1}$ for $[Mn^{II}L](ClO_4)_2$, 286 $mol^{-1}\,cm^2\,\Omega^{-1}$ for $[Fe^{II}L](BF_4)_2$ and 301 $mol^{-1}\,cm^2\,\Omega^{-1}$ for $[Ni^{II}L](BF_4)_2$ in acetonitrile indicate that all three cryptates behave as 2:1 electrolytes in solution.

The UV/Vis spectrum of yellow $[Mn^{II}L](ClO_4)_2$ in acetonitrile shows strong ligand-centred π-π* transitions at 208 nm (ε = 62100 $M^{-1}\,cm^{-1}$) and 250 nm (ε = 35100 $M^{-1}\,cm^{-1}$), with a lower intensity shoulder tailing off to longer wavelengths. The UV/Vis spectrum of $[Fe^{II}L](BF_4)_2$ in acetonitrile shows a band of at least four overlapping metal-to-ligand charge-transfer transitions with distinct peaks at 428 nm (ε = 4800 $M^{-1}\,cm^{-1}$) and 588 nm (ε = 8030 $M^{-1}\,cm^{-1}$) and shoulders at 370 nm and 540 nm. There are also transitions at 213 nm (ε = 64700 $M^{-1}\,cm^{-1}$) and a shoulder at about 250 nm which are probably due to ligand-centred π-π* transitions. The UV/Vis spectrum of $[Ni^{II}L](BF_4)_2$ in acetonitrile shows a band of overlapping weak d-d transitions (ε ≈ 30 $M^{-1}\,cm^{-1}$) with maxima at 825 and 908 nm. This is consistent with the presence of octahedral nickel(II). A second band at 211 nm (ε = 68700 $M^{-1}\,cm^{-1}$) with a shoulder at about 250 nm is assigned to ligand-centred π-π* transitions.

The ^1H NMR spectrum of $[Fe^{II}L](BF_4)_2$ at 243 K (Figure 2) is consistent with the existence of an unsymmetrical cryptate with the low spin iron(II) ion being located in one tren-derived cap site of the cryptand. The three strands are identical as expected. Each methylene group is differentiated into an axial triplet and equatorial doublet signal as a result of the accidental similarity of the geminal $^2J_{ax/eq}$ and vicinal $^3J_{ax/ax'}$ coupling constants of ca. 11−13 Hz (cf. 11−12 Hz for L).[9] Two-dimensional correlation NMR spectroscopic techniques were used to identify the signals for each end of the cryptand. The two ends of the cryptand were tentatively assigned by comparison with the $[ZnL](ClO_4)_2$ and $[Fe^{II}Cu^{I}L]^{3+}$ spectra and on the basis that the signals for the protons at end of the cryptand containing iron(II) are expected to be more deshielded due to the lower electron density in this half of the cryptand. It is worth noting that if this latter point is incorrect (and there are some inconsistencies in the carbon NMR spectrum), then the 'end' assignments would need to be reversed. At higher temperatures the ^1H NMR spectrum of $[Fe^{II}L](BF_4)_2$ shows significant changes, with the signals for the end of the cryptand which is believed to contain the iron(II) ion shifting, broadening or disappearing altogether as the

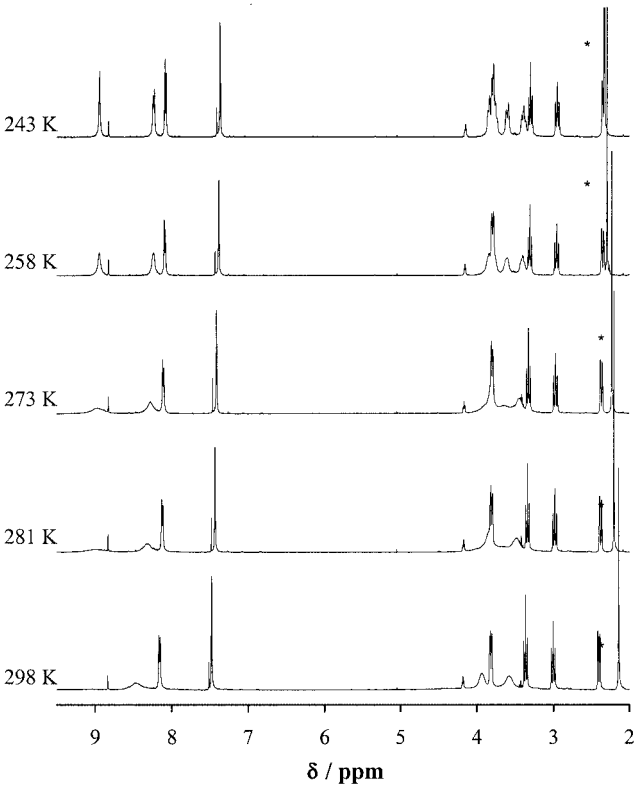

Figure 2. Variable temperature ^1H NMR spectra of $[Fe^{II}L](BF_4)_2$ in CD_3CN; the strong signal to the right hand side of the asterisk * is H_2O; note that the spectra at 273 K and 281 K were recorded on a different sample to the other spectra

temperature is raised to 298 K (Figure 2). The signals for the other half of the cryptand remain sharp at all temperatures examined. This type of behaviour is characteristic of paramagnetic compounds, suggesting the existence of an equilibrium involving at least a small amount of high spin Fe^{II}. The broadening and shifting become more severe as the temperature is increased, in accordance with Curie-law behaviour. Another possibility that this temperature-dependent behaviour is simply due to fluxionality in the uncoordinated 'end' is believed to be unlikely on the basis that (a) the ^1H NMR spectrum of $[ZnL](ClO_4)_2$ is sharp at room temperature, (b) it would require the 'end' assignments to be reversed, and (c) whilst at first glance the H^{9a}/H^{9b} and H^{10a}/H^{10b} pairs of alkyl signals each appear to coalesce into two broad signals, for H^9 and H^{10}, respectively, at higher temperatures (δ = 3.94 and 3.59 ppm at 298 K), the position of these signals is not exactly at the averaged position (e.g. see relative positions of $H^{10a+10b}/H^{10}$ vs. H^{7b} as a function of temperature) and more seriously the integration is not correct as each broad signal integrates as equivalent to only one proton (not two). Finally, the H^{11} and H^3 signals shift as well as broaden.

The previous synthesis of $[Cu^I_2L](BF_4)_2$ and $[Ag^I_2L](ClO_4)_2$[9,10] suggested that it should be possible to synthesise homodinuclear cryptates of other non-stereochemically demanding metal ions.

The addition of two equivalents of zinc perchlorate to L in acetonitrile resulted in the dinuclear cryptate $[Zn_2L](ClO_4)_4$. The IR spectrum of $[Zn_2L](ClO_4)_4$ confirms that the cryptand is intact with an imine band at 1653 cm^{-1}. The bands for the ClO_4^- counterions, centred around 1121 cm^{-1} and 629 cm^{-1}, are both clearly split into three peaks indicating that there may be some interaction with the $[Zn_2L]^{4+}$ cation which lowers the symmetry of the ClO_4^- ion. The electrospray mass spectrum of $[Zn_2L](ClO_4)_4$ only shows peaks for the mononuclear species $[ZnL]^{2+}$ and $[ZnL](ClO_4)^+$. The elemental analysis, however, fits the dinuclear formulation. The UV/Vis spectrum of yellow $[Zn_2L](ClO_4)_4$ in acetonitrile shows transitions at 206 nm (ε = 51900 $M^{-1}\,cm^{-1}$) and 251 nm (ε = 30400 $M^{-1}\,cm^{-1}$) with lower intensity shoulders tailing to longer wavelengths.

The conductivity measurement of 359 $mol^{-1}\,cm^2\,\Omega^{-1}$ in acetonitrile is consistent with the complex being a 3:1 electrolyte (3:1, 340−420 $mol^{-1}\,cm^2\,\Omega^{-1}$)[12] instead of a 4:1 electrolyte as expected. The lower than expected conductivity value may well be a consequence of the reduced mobility often observed for large polycations,[12] although the 3:1 electrolyte cryptates described here have conductivity values within the expected ranges. Another, less likely, explanation is that it might be due to the symmetrical (see NMR spectrum later) coordination of one of the ClO_4^- counterions to the two zinc ions in solution. This would be consistent with the split ClO_4^- bands observed in the solid-state infrared spectrum (KBr disc), however, it would require a very different binding arrangement to those observed for all of the complexes of L studied to date, and such a bridging arrangement of the anion would also be unique for an imine, as opposed to amine, cryptand.[1] An X-ray structure determination would be required to test the latter hypothesis; however, the crystals of $[Zn_2L](ClO_4)_4$ obtained from acetonitrile were not of X-ray quality. Attempts to synthesise the BF_4^- analogue of $[Zn_2L](ClO_4)_4$ were unsuccessful, suggesting that the presence of ClO_4^- is necessary to form the dinuclear complex.

An attempted synthesis of $[Zn_2L](ClO_4)_4$ in methanol and a recrystallisation of $[Zn_2L](ClO_4)_4$ from dimethylformamide (DMF) both resulted in the mononuclear cryptate $[ZnL](ClO_4)_2$ in a slightly impure form. The NMR spectra of this mononuclear zinc complex in CD_3CN are sharp, in direct contrast to the broad and temperature-dependent ^1H NMR spectra obtained for $[Fe^{II}L](BF_4)_2$, and are consistent with an unsymmetrical cryptate in which the zinc(II) ion is located in one tren-derived cap site of the cryptand (see Exp. Sect. and Supporting Information). As expected, the ^1H NMR spectrum of the dinuclear zinc complex, $[Zn_2L](ClO_4)_4$, in CD_3CN is simple due to its high symmetry, with just one resonance for the imine protons and one for the aromatic protons, together with the expected two sets of axial and equatorial resonances for the tren-derived caps. This shows that in acetonitrile solution the dinuclear cryptate is stable with respect to the mononuclear analogue. Thus, the use of acetonitrile as the solvent also appears to be crucial for the stability of the dinuclear complex $[Zn_2L](ClO_4)_4$.

Further attempts to synthesise homodinuclear cryptates were carried out with the non-stereochemically demanding cations manganese(II) and sodium ions and resulted in $Mn^{II}_2LCl_4\cdot H_2O$ and $[Na_2L](CF_3SO_3)_2$, respectively, in the analytically pure form. Interestingly the conductivity value for $Mn^{II}_2LCl_4\cdot H_2O$ (224 $mol^{-1}\,cm^2\,\Omega^{-1}$ in methanol) is closest to that for a 2:1 electrolyte (ref. 2:1: 160−220 $mol^{-1}\,cm^2\,\Omega^{-1}$, 3:1: 290−350 $mol^{-1}\,cm^2\,\Omega^{-1}$)[12] rather than a 4:1 electrolyte initially expected. This suggests that either two of the chloride anions are coordinated to the manganese(II) ions in the dimanganese cryptate, either in a monodentate or bridging fashion, or that a monomanganese cryptate with a $[MnCl_4]^{2-}$ counterion has formed. The latter of these possibilities is not supported by negative ion mass spectrometry as this shows no evidence for the presence of $[MnCl_4]^{2-}$. Attempts to grow single crystals of $Mn^{II}_2LCl_4\cdot H_2O$ and $[Na_2L](CF_3SO_3)_2$, suitable for X-ray diffraction, were unsuccessful.

The addition of two equivalents of manganese(II) perchlorate to L resulted only in the mononuclear cryptate $[Mn^{II}L](ClO_4)_2$ (described above). Thus, although it appears to be possible to synthesise dinuclear cryptates of L with non-stereochemically demanding divalent cations, the choice of counterion and/or solvent appears to be crucial.

Synthesis and Characterisation of Heterodinuclear Cryptates

The previous synthesis of $[Co^{II}Cu^{I}L](BF_4)_3$ and $[Cu^{II}Cu^{I}L](BF_4)_3$[8] suggested that it should be possible to synthesise other heterodinuclear cryptates of L by the addition of a non-stereochemically demanding cation to the

mononuclear cryptates $[M^{II}L](X)_2$ (M = Mn, Fe, Ni; X = BF_4^- or ClO_4^-). The heterodinuclear cryptates $[Mn^{II}Cu^{I}L](ClO_4)_2(BF_4)$, $[Fe^{II}Cu^{I}L](BF_4)_3{\cdot}CH_3CN$ and $[Ni^{II}Cu^{I}L](BF_4)_3{\cdot}H_2O$ were synthesised by the addition of one equivalent of an appropriate salt of the divalent cation followed by the addition of $Cu^{I}(CH_3CN)_4BF_4$. This one-pot approach is analogous to that used to synthesise the heterodinuclear cryptate $[Co^{II}Cu^{I}L](BF_4)_3$, except that acetonitrile was used as the solvent instead of methanol. The synthesis of $[Mn^{II}Cu^{I}L](ClO_4)_2(BF_4)$ required the addition of 1.1 equivalents of $Cu^{I}(CH_3CN)_4BF_4$ to avoid the formation of a yellow by-product proposed to be $[Mn^{II}L](ClO_4)_2$. The cryptates $[Mn^{II}Cu^{I}L](ClO_4)_2(BF_4)$ and $[Ni^{II}Cu^{I}L](BF_4)_3{\cdot}H_2O$ were isolated in good yield and purity by diethyl ether diffusion into the acetonitrile reaction mixtures. When this approach was used to isolate $[Fe^{II}Cu^{I}L](BF_4)_3{\cdot}CH_3CN$ a green crystalline by-product, apparently $[Cu^{II}L](BF_4)_2$, resulted. The production of this by-product was avoided by precipitating the product from the reaction mixture and recrystallising the crude product from acetonitrile by diethyl ether diffusion. The success of this strategy suggests that once formed there is no significant dissociation of the heterodinuclear cryptate in this case. The elemental analyses of all three complexes were consistent with their proposed formulae, with the metal analyses providing additional evidence of the presence of the two different metal ions.

Imine bands (and the absence of amine or carbonyl absorptions) in the infrared spectra of these heterodinuclear cryptates confirms that the L cryptand remains intact {1652 cm^{-1} for $[Mn^{II}Cu^{I}L](ClO_4)_2(BF_4)$, 1635 cm^{-1} for $[Fe^{II}Cu^{I}L](BF_4)_3{\cdot}CH_3CN$ and 1636 cm^{-1} for $[Ni^{II}Cu^{I}L](BF_4)_3{\cdot}H_2O$}. The infrared spectra of $[Fe^{II}Cu^{I}L](BF_4)_3{\cdot}CH_3CN$ and $[Ni^{II}Cu^{I}L](BF_4)_3{\cdot}H_2O$ show bands for the tetrafluoroborate counterions at 1083 cm^{-1}. The infrared spectrum of $[Mn^{II}Cu^{I}L](ClO_4)_2(BF_4)$ confirms the presence of both counterions with bands at 1117 cm^{-1} for ClO_4^- and 1083 cm^{-1} for BF_4^-.

The mass spectra of the three heterodinuclear cryptates confirm the presence of both metal ions with peaks observed for the mixed-metal clusters [MCuL] (M = Mn, Fe, Ni) in all cases. There is no evidence in any of the mass spectra for homodinuclear species of the type $[M_2L]$ or $[Cu_2L]$.

The conductivity values of 407 $mol^{-1}\,cm^2\,\Omega^{-1}$ for $[Mn^{II}Cu^{I}L](ClO_4)_2(BF_4)$, 393 $mol^{-1}cm^2\Omega^{-1}$ for $[Fe^{II}Cu^{I}L](BF_4)_3{\cdot}CH_3CN$ and 403 $mol^{-1}\,cm^2\,\Omega^{-1}$ for $[Ni^{II}Cu^{I}L](BF_4)_3{\cdot}H_2O$ indicate that all three cryptates behave as 3:1 electrolytes in acetonitrile solution.

The UV/Vis spectrum of $[Mn^{II}Cu^{I}L](ClO_4)_2(BF_4)$ has a band at 250 nm (ε = 33000 $M^{-1}\,cm^{-1}$) which is assigned to ligand-centred π-π^* transitions and is similar to that observed in the mononuclear cryptates and the free ligand L. This band has a broad shoulder at about 280 nm. No band corresponding to charge transfer transitions of the copper(I) ion can be clearly distinguished. The UV/Vis spectrum of $[Fe^{II}Cu^{I}L](BF_4)_3{\cdot}CH_3CN$ shows a group of at least four overlapping transitions with distinct peaks at 443 nm (ε = 10700 $M^{-1}\,cm^{-1}$) and 557 nm (ε = 10500 $M^{-1}\,cm^{-1}$) and shoulders at 390 nm and 540 nm. These transitions, which obscure any possible Cu^{I} MLCT band, are similar to those seen for $[Fe^{II}L](BF_4)_2$. There is also a strong π-π^* transition at 211 nm (ε = 75000 $M^{-1}\,cm^{-1}$) with a very broad shoulder extending out to 300 nm. The UV/Vis spectrum of $[Ni^{II}Cu^{I}L](BF_4)_3{\cdot}H_2O$ shows a band of weak d-d transitions ($\varepsilon \approx 20\ M^{-1}\,cm^{-1}$) with a peak at 806 nm. This is similar to the UV/Vis spectrum of $[Ni^{II}L](BF_4)_2$ and is consistent with the presence of octahedral nickel(II). There is also an additional band at 413 nm (ε = 2510 $M^{-1}\,cm^{-1}$) which is assigned to charge-transfer transitions of the copper(I) ion and is similar to that observed in $[Cu^{I}_2L](BF_4)_2$ (390 nm, ε = 3960 $M^{-1}\,cm^{-1}$).[10] Finally, a shoulder, due to ligand-centred π-π^* transitions, is observed at 250 nm.

The magnetic moments of 5.9 BM for $[Mn^{II}Cu^{I}L](ClO_4)_2(BF_4)$ and 3.1 BM for $[Ni^{II}Cu^{I}L](BF_4)_3{\cdot}H_2O$ are consistent with the presence of the spin-free paramagnetic divalent cation and the d^{10} copper(I) ion. The complex $[Fe^{II}Cu^{I}L](BF_4)_3{\cdot}CH_3CN$ was determined to be diamagnetic, which is consistent with the presence of low spin iron(II) and copper(I). The ^1H NMR spectrum of $[Fe^{II}Cu^{I}L](BF_4)_3{\cdot}CH_3CN$ (Figure 3) at 298 K shows sharp peaks, further confirming the diamagnetic nature of this complex. The spectrum is similar to that of $[ZnL](ClO_4)_2$ in that it is sharp and lacks end-to-end symmetry, and broadly similar to that of $[Fe^{II}L](BF_4)_2$, except that there is no broadening at room temperature and $^3J_{eq/eq}$ (ca. 4 Hz) coupling is observed. These observations, together with the absence of dissociation in solution noted earlier, indicate a regular octahedral site for the Fe^{II} ion in the $[Fe^{II}Cu^{I}L](BF_4)_3{\cdot}CH_3CN$ cryptate.

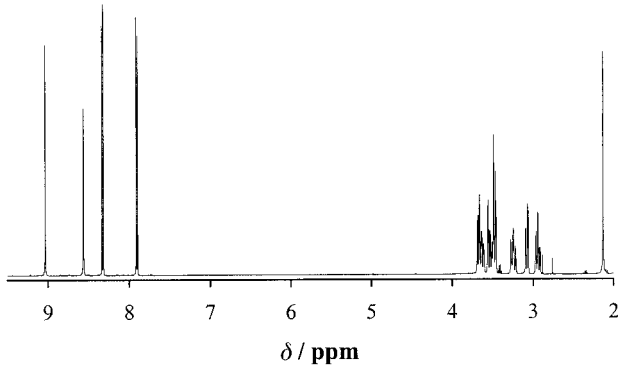

Figure 3. ^1H NMR spectrum of $[Fe^{II}Cu^{I}L](BF_4)_3{\cdot}CH_3CN$ at 298 K in CD_3CN

Crystal Structures of Mononuclear Cryptates

Single crystals of the mononuclear cryptates $[Mn^{II}L](ClO_4)_2$, $[Fe^{II}L](BF_4)_2$ and $[Ni^{II}L](ClO_4)_2$ were obtained by diethyl ether diffusion into dimethylformamide, acetonitrile and acetonitrile solutions of the cryptates, respectively, and the crystal structures were determined by X-ray diffraction techniques.

The d^5 manganese(II) ion in each of the two independent $[Mn^{II}L]^{2+}$ cryptates in the asymmetric unit is seven coordi-

nate as a consequence of binding to three imine nitrogen atoms, three pyridazine nitrogen atoms and the bridgehead nitrogen atom (Figure 4, Table 1). However, the interaction with the bridgehead nitrogen atom is comparatively weak [av. $Mn-N_{imine}$ = 2.209 Å, av. $Mn-N_{pyridazine}$ = 2.384 Å, av. $Mn-N_{bridgehead}$ = 2.524 Å]. The $N_{bridgehead}\cdots N_{bridgehead}$ distance [N(4)···N(5) = 10.236(5) Å, N(54)···N(55) = 10.311(5) Å] is short in comparison with the free cryptand [10.443(7) Å].[9]

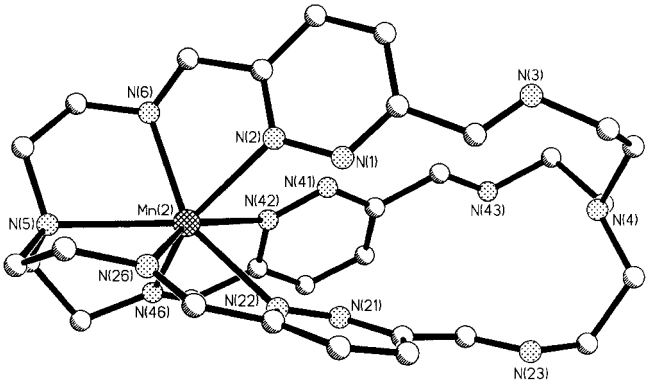

Figure 4. Perspective view of one of the two unique $[Mn^{II}L]^{2+}$ cations of $[Mn^{II}L](ClO_4)_2$; hydrogen atoms have been omitted for clarity

The structure of $[Ni^{II}L](ClO_4)_2$ is very similar to that of $[Co^{II}L]^{2+}$.[9] The nickel(II) ion in each of the two independent cryptates in the asymmetric unit is six coordinate as a consequence of binding to three imine nitrogen atoms and three pyridazine nitrogen atoms (Figure 5, Table 1). The twist angle (φ) of the nickel(II) ion [46.4° for Ni(2) and 47.0° for Ni(52)] indicates a distorted octahedral geometry (φ = 60° for octahedral and 0° for trigonal prismatic).[1] This is very similar to the twist angle of 46.9° seen for the cobalt(II) ion in $[Co^{II}L]^{2+}$.[9] The coordination of the nickel ion does not change the $N_{bridgehead}\cdots N_{bridgehead}$ distance of the cryptand by much [N(4)···N(5) = 10.519(9) Å, N(54)···N(55) = 10.421(9) Å; L 10.443(7) Å].

The structure of $[Fe^{II}L](BF_4)_2$ is similar to that of the above mononuclear cryptates, however, as the X-ray analysis is of poor quality, it is not discussed further (see Supporting Information).

The structures of $[M^{II}L]^{2+}$ (M = Mn, Fe, Co, Ni, Cu) indicate that L is able to accommodate a single, relatively stereochemically demanding, cation in geometries ranging from five to seven coordinate, although six coordination is the most common. In all of these mononuclear cryptates, all three of the strands of the organic host have all *trans* conformations. These strands would therefore have to change their conformations to all *cis* before a second metal cation could bind.

Crystal Structures of Heterodinuclear Cryptates

Single crystals of the heterodinuclear cryptates $[Mn^{II}Cu^{I}L](ClO_4)_2(BF_4)$, $[Fe^{II}Cu^{I}L](BF_4)_3{\cdot}2.5CH_3CN$ and $[Ni^{II}Cu^{I}L](BF_4)_3$ were obtained by the slow diffusion of diethyl ether vapour into acetonitrile solutions of the cryptates. A summary of key crystallographic information is given in Figures 6, 7, 8 and Tables 1−2. The structures of $[Mn^{II}Cu^{I}L]^{3+}$ and $[Ni^{II}Cu^{I}L]^{3+}$ are end-for-end disordered, as was the case in the previously determined structure of $[Co^{II}Cu^{I}L]^{3+}$ with the three strands of the cryptand also disordered in order to accommodate the differing coordination geometries of the two different metal cations.[8] Unless otherwise stated, only the major occupancy forms of each cryptate will be discussed. The structure of $[Fe^{II}Cu^{I}L]^{3+}$ is the first structure of a heterodinuclear cryptate of L that is not end-for-end disordered.

The structures of $[Mn^{II}Cu^{I}L]^{3+}$, $[Ni^{II}Cu^{I}L]^{3+}$ and $[Fe^{II}Cu^{I}L]^{3+}$ are similar to each other. In all cases, the divalent cation is six-coordinate and binds to three pyridazine and three imine nitrogen atoms. This is also observed in the previously reported heterodinuclear cryptate $[Co^{II}Cu^{I}L]^{3+}$ and the mixed-valent cryptate $[Cu^{II}Cu^{I}L]^{3+}$.[8]

Of all the $[M^{II}Cu^{I}L]^{3+}$ cryptates (M = Mn, Co, Fe, Ni, Cu), the geometry of the iron(II) ion in $[Fe^{II}Cu^{I}L]^{3+}$ is closest to a regular octahedron indicating that iron(II) is the most stereochemically demanding cation. Here the twist angle (φ) of the iron(II) ion within the N_6 donor set is 50.4°. In contrast, the twist angle of the manganese(II) ion in $[Mn^{II}Cu^{I}L]^{3+}$ [35.9° for Mn(2)] indicates that the geometry is intermediate between octahedral and trigonal prismatic. This is significantly different from the more octahedral geometries observed for the six-coordinate cryptates $[Co^{II}L]^{2+}$, $[Ni^{II}L]^{2+}$ and $[M^{II}Cu^{I}L]^{3+}$ (M = Fe, Co, Ni, Cu), where the twist angles range from 45.4−50.4° (Table 2). However, this is consistent with manganese(II) being less stereochemically demanding than the other divalent cations as a result of its d^5 configuration. The greater deviation from regular octahedral geometry for manganese(II) in $[Mn^{II}Cu^{I}L]^{3+}$ is also reflected in the wider range of *cis* N−M−N angles (71.5−105.4° for Mn(2) compared with 80.7−97.0° for Fe(2) in $[Fe^{II}Cu^{I}L]^{3+}$) (Table 2).

The non-stereochemically demanding copper(I) ion in $[Mn^{II}Cu^{I}L]^{3+}$, $[Ni^{II}Cu^{I}L]^{3+}$ and $[Fe^{II}Cu^{I}L]^{3+}$ has a distorted trigonal-pyramidal geometry and is coordinated by three imine nitrogen atoms and the bridgehead nitrogen atom. However, the interactions with the imine nitrogen atoms are stronger than those with the bridgehead nitrogen atoms [av. $Cu(1)-N_{imine}$ = 2.00 Å, $Cu(1)-N_{bridgehead}$ = 2.33 Å] (Table 2). The copper(I) ion is displaced from the mean plane of the three imine nitrogen donors towards the centre of the cavity by 0.24−0.31 Å (Table 2), that is, away from the bridgehead nitrogen atom. This is also seen in the structure of the dicopper(I) cryptate $[Cu^{I}_2L](BF_4)_2$, where the two copper(I) ions are displaced from their $(N_{imine})_3$ mean planes, away from the bridgehead nitrogen atoms, by 0.238 and 0.234 Å, respectively,[10] and in the structures of other tren-derived Schiff-base cryptates.[13] Thus, although the copper(I) ions are within bonding distance of the bridgehead nitrogen atom, this interaction is primarily due to their enforced proximity. The distances between Cu(1) and the pyridazine nitrogen atoms {for example, in $[Fe^{II}Cu^{I}L]^{3+}$, shortest $Cu-N_{pyridazine}$ distance is 3.007 Å,

Table 1. Selected bond lengths [Å] and bond angles [°] for mononuclear and heterodinuclear cryptates of L

	$[Mn^{II}L]^{2+}$ [a]	$[Ni^{II}L]^{2+}$ [a]	$[Mn^{II}Cu^{I}L]^{3+}$ [b]	$[Fe^{II}Cu^{I}L]^{3+}$	$[Ni^{II}Cu^{I}L]^{3+}$ [c]
Cu(1)−N(3)			2.020(3)	2.002(3)	1.993(2)
Cu(1)−N(23)			2.068(3)	1.998(3)	2.003(2)
Cu(1)−N(43)			2.037(3)	2.010(3)	1.970(2)
Cu(1)−N(4)			2.298(3)	2.332(3)	2.365(3)
M(2)−N(46)	2.206(3)	2.116(5)	2.176(3)	1.966(3)	2.138(2)
M(2)−N(26)	2.205(3)	2.088(5)	2.251(3)	1.962(3)	2.136(2)
M(2)−N(6)	2.204(3)	2.108(5)	2.288(3)	1.971(3)	2.095(2)
M(2)−N(22)	2.405(3)	2.129(5)	2.315(4)	1.928(3)	2.067(3)
M(2)−N(42)	2.349(3)	2.103(5)	2.342(4)	1.937(3)	2.087(3)
M(2)−N(2)	2.369(3)	2.117(5)	2.360(4)	1.931(3)	2.070(3)
M(2)−N(5)	2.524(3)				
N(3)−Cu(1)−N(23)			117.62(12)	119.00(13)	116.95(10)
N(3)−Cu(1)−N(43)			121.69(12)	115.64(12)	115.83(10)
N(23)−Cu(1)−N(43)			114.38(12)	118.95(12)	119.59(10)
N(3)−Cu(1)−N(4)			82.47(10)	81.49(13)	80.71(9)
N(23)−Cu(1)−N(4)			81.20(11)	81.75(12)	80.11(9)
N(43)−Cu(1)−N(4)			81.09(11)	81.32(12)	81.39(10)
N(46)−M(2)−N(26)	111.21(11)	103.22(19)	105.44(12)	95.84(14)	100.13(9)
N(46)−M(2)−N(6)	110.35(11)	100.78(18)	103.86(11)	95.05(14)	96.72(9)
N(26)−M(2)−N(6)	111.41(11)	101.66(19)	100.11(11)	96.96(14)	102.20(9)
N(46)−M(2)−N(22)	94.85(10)	95.24(18)	103.60(13)	92.21(13)	93.93(10)
N(26)−M(2)−N(22)	70.39(10)	77.6(2)	73.12(13)	80.80(13)	76.65(10)
N(6)−M(2)−N(22)	150.80(10)	163.64(18)	152.54(14)	172.59(14)	169.31(10)
N(46)−M(2)−N(42)	71.02(11)	77.80(18)	72.68(13)	80.66(13)	77.63(10)
N(26)−M(2)−N(42)	150.78(11)	164.33(19)	156.82(16)	171.07(13)	167.49(10)
N(6)−M(2)−N(42)	93.74(11)	93.42(18)	102.76(14)	91.55(12)	90.30(10)
N(22)−M(2)−N(42)	80.40(10)	86.72(19)	84.74(16)	91.09(12)	91.16(11)
N(46)−M(2)−N(2)	151.09(11)	162.76(18)	157.08(16)	169.79(13)	163.90(10)
N(26)−M(2)−N(2)	93.74(10)	93.86(18)	97.48(14)	93.98(13)	95.84(10)
N(6)−M(2)−N(2)	71.26(10)	77.63(18)	71.54(12)	80.94(13)	77.80(10)
N(22)−M(2)−N(2)	79.55(10)	86.09(18)	82.81(15)	92.13(12)	91.70(11)
N(42)−M(2)−N(2)	80.07(10)	85.13(18)	86.25(16)	90.02(12)	87.19(11)
N(6)−M(2)−N(5)	71.99(10)				
N(26)−M(2)−N(5)	71.99(10)				
N(46)−M(2)−N(5)	72.31(10)				
N(42)−M(2)−N(5)	132.47(9)				
N(2)−M(2)−N(5)	131.74(10)				
N(22)−M(2)−N(5)	132.00(10)				

[a] Data for one of the two unique cations in the asymmetric unit. [b] Data for major occupancy cryptate. [c] Data for major occupancy cryptate of one of the two unique cations in the asymmetric unit.

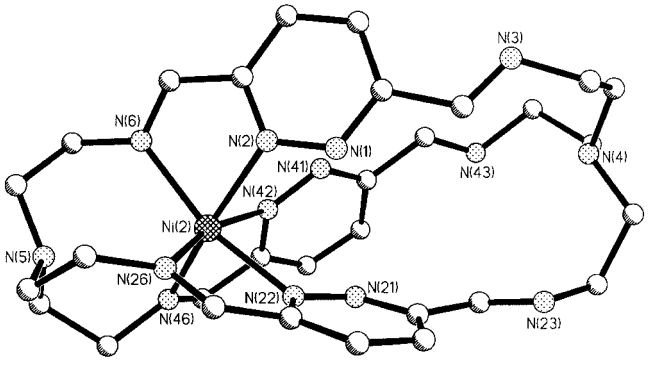

Figure 5. Perspective view of one of the two unique $[Ni^{II}L]^{2+}$ cations of $[Ni^{II}L](BF_4)_2$; hydrogen atoms have been omitted for clarity

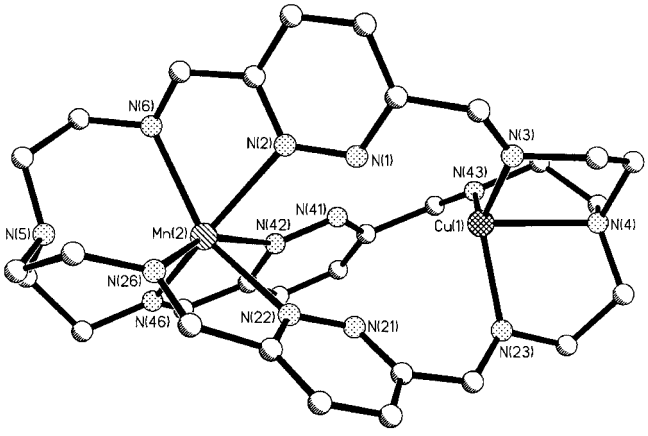

Figure 6. Perspective view of the major occupancy form of the $[Mn^{II}Cu^{I}L]^{3+}$ cation of $[Mn^{II}Cu^{I}L](ClO_4)_2(BF_4)$; hydrogen atoms have been omitted for clarity

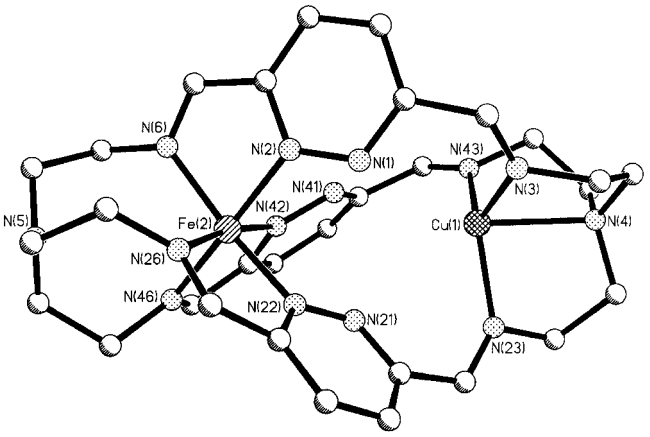

Figure 7. Perspective view of the cation $[Fe^{II}Cu^{I}L]^{3+}$ of $[Fe^{II}Cu^{I}L](BF_4)_3{\cdot}CH_3CN$; hydrogen atoms have been omitted for clarity

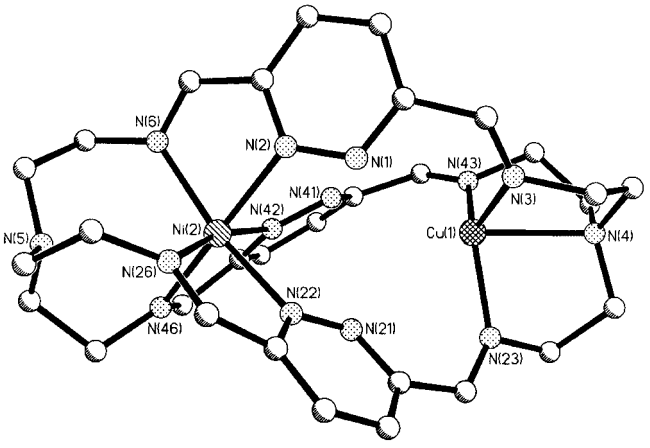

Figure 8. Perspective view of the major occupancy form of one of the two unique $[Ni^{II}Cu^{I}L]^{3+}$ cations of $[Ni^{II}Cu^{I}L](BF_4)_3{\cdot}H_2O$; hydrogen atoms have been omitted for clarity

for Cu(1)−N(41)} preclude further strong bonding interactions. In all cases, the geometry of the copper ion is consistent with the proposed +1 oxidation state.

In the series of heterodinuclear cryptates, the $M^{II}\cdots Cu^{I}$ interatomic distance follows the order Mn > Co > Cu > Ni > Fe (Table 2), decreasing with the decreasing ionic radius of the divalent cation.[14] This order is also weakly correlated to the trigonal prismatic twist angle φ, with Mn having the smallest (36°) and Fe the largest (50°) twist angle. The trend in $N_{bridgehead}\cdots N_{bridgehead}$ distances is less clear, although $[Fe^{II}Cu^{I}L]^{3+}$, which has the shortest $M^{II}\cdots Cu^{I}$ interatomic distance of 4.723(6) Å, also has the shortest $N_{bridgehead}\cdots N_{bridgehead}$ distance of 10.059(6) Å (Table 2). Conversely, the manganese cryptate $[Mn^{II}Cu^{I}L]^{3+}$ has the longest $M^{II}\cdots Cu^{I}$ interatomic distance of 5.231(10) Å and the longest $N_{bridgehead}\cdots N_{bridgehead}$ distance of 10.455(10) Å.

The structures of $[Mn^{II}Cu^{I}L]^{3+}$and $[Ni^{II}Cu^{I}L]^{3+}$ show both differences and similarities to the structures of the corresponding mononuclear cryptates $[Mn^{II}L]^{2+}$ and $[Ni^{II}L]^{2+}$. In both heterodinuclear cases, the L cryptand has adopted a conformation with mutually *cis* imino C=N functions in each strand in order to bind the copper(I) ions. This is in contrast to the mutually *trans* conformations seen in the corresponding mononuclear cryptates. For $[Mn^{II}Cu^{I}L]^{3+}$, the binding of copper(I) has also altered the coordination geometry of the manganese(II) ion, reducing its coordination number from seven to six as a result of a lengthening of the $Mn-N_{bridgehead}$ distance from 2.524(3) Å in $[Mn^{II}L]^{2+}$ to 2.931(6) Å in $[Mn^{II}Cu^{I}L]^{3+}$. Coordination of the copper(I) ion has also increased the overall length of the cryptand. The $N_{bridgehead}\cdots N_{bridgehead}$ distance is 10.455(10) Å for Mn(1) in $[Mn^{II}Cu^{I}L]^{3+}$ and 10.236(5) Å for $[Mn^{II}L]^{2+}$. The distorted octahedral geometry of the nickel(II) ion in $[Ni^{II}Cu^{I}L]^{3+}$ is similar to that seen in the mononuclear nickel(II) cryptate $[Ni^{II}L]^{2+}$. The twist angles of nickel(II) [47.2° for Ni(2) and 47.3° for Ni(3)] are very similar to that seen in $[Ni^{II}L]^{2+}$. The N···N bridgehead distances [10.309(6) and 10.413(6) Å for the two unique cations] are slightly shorter than those of $[Ni^{II}L]^{2+}$ [10.519(9) and 10.421(9) Å for the two unique cations].

The cryptate $[Fe^{II}Cu^{I}L]^{3+}$ is of some interest as a structural model for the oxygen binding site of cytochrome c oxidase. This dinuclear site consists of a heme a_3 iron and a copper ion (Cu_B) with an interatomic distance of 4.5−5.2 Å depending on the source of the enzyme.[15] The cation $[Fe^{II}Cu^{I}L]^{3+}$ has a similar Fe···Cu interatomic distance to cytochrome c oxidase with the same oxidation states present as in the fully reduced form of the enzyme. However, the iron(II) ion in $[Fe^{II}Cu^{I}L]^{3+}$ has more donor atoms than the

Table 2. Comparison of X-ray crystallographic data for heterodinuclear cryptates of L

Compound	φ(M^{2+}) [°]	Range of *cis* N−M−N angles [°]	$M^{II}\cdots Cu^{I}$ [Å]	Bridgehead distance [Å]	$Cu-N_{bridgehead}$ [Å]	Av. $Cu-N_{imine}$ [Å]	Cu displacement from $(N_{imine})_3$ plane [Å]
$[Mn^{II}Cu^{I}L]^{3+}$ [a]	35.9	71.5−105.4	5.231(10)	10.455(10)	2.298(3)	2.042	0.298
$[Fe^{II}Cu^{I}L]^{3+}$	50.4	80.7−97.0	4.723(6)	10.059(6)	2.332(3)	2.003	0.295
$[Co^{II}Cu^{I}L]^{3+}$ [b]	47	73.2−111.5	5.08(1)	10.159(14)	2.292(5)	1.996	0.324
$[Ni^{II}Cu^{I}L]^{3+}$ [c]	47.2	76.7−102.2	4.821(9)	10.309(6)	2.365(3)	1.989	0.320
	47.3	78.4−99.4	4.904(9)	10.413(6)	2.322(3)	1.949	0.242
$[Cu^{II}Cu^{I}L]^{3+}$ [b]	45.4	74.5−103.4	4.960(2)	10.306(8)	2.330(10)	2.001	0.27

[a] Data for the major occupancy cryptate. [b] Data from reference.[8] [c] Data for the major occupancy cryptates of the two unique cations in the asymmetric unit.

Table 3. Summary of electrochemical data for cryptates of L

Compound	$E_{1/2}$ (ΔE)[a]									
$[Mn^{II}L]^{2+}$			−1.76 (0.08)	−1.49 (0.07)	−1.24 (0.08)			+1.03^{I}		
$[Fe^{II}L]^{2+}$			−1.87 (0.11)^{QR}	−1.42 (0.07)	−1.13 (0.07)	+0.78^{QR} [b]	+0.86^{QR} [b]			
$[Co^{II}L]^{2+}$ [c]			−1.71^{QR}	−1.56 (0.08)	−1.14 (0.07)	+0.29 (0.13)^{QR}	+0.95^{I}	+1.09^{I}	+1.34^{I}	+1.57^{I}
$[Ni^{II}L]^{2+}$			−1.88 (0.07)^{QR}	−1.34 [b]	−1.25[b]		+0.99^{I}	+1.05^{I}	+1.34^{I}	
$[Cu^{II}L]^{2+}$ [d],[e]				−1.75^{QR}	−1.37^{QR}	−0.38 (0.08)	+1.00^{I}	+1.16^{I}		
$[Mn^{II}Cu^{I}L]^{3+}$		−1.89^{QR} [b]	−1.77^{QR} [b]	−1.46 (0.09)	−1.25 (0.08)	−0.86^{I}	+0.25 (0.10)^{QR}	+0.81^{QR}	+1.07^{I}	
$[Fe^{II}Cu^{I}L]^{3+}$		−1.89^{QR}	−1.55 (0.07)	−1.27 (0.07)	−1.07 (0.09)		+0.49 (0.10)	+0.97^{I}	+1.11^{I}	
$[Co^{II}Cu^{I}L]^{3+}$		−1.55 (0.08)^{QR}	−1.41 (0.10)^{QR}	−1.15 (0.07)^{QR}	−0.88 (0.06)^{QR}	+0.08^{QR} [f]	+0.58^{QR} [f]	+1.07^{I}	+1.33^{I}	+1.63^{I}
$[Ni^{II}Cu^{I}L]^{3+}$		−1.89^{QR}	−1.53 (0.08)	−1.36^{QR}	−1.19 (0.12)		+0.46 (0.07)	+1.07^{I}	+1.34^{I}	
$[Cu^{II}Cu^{I}L]^{3+}$ [d]			−1.98^{QR}	−1.44^{QR}	−1.27^{QR}	−0.34 (0.08)	+0.33 (0.08)	+1.18^{I}		
$[Zn^{II}{}_2L]^{4+}$	−1.73^{QR}	−1.62^{QR}	−1.10 (0.07)	−0.95 (0.06)	−0.84 (0.06)			+1.30^{I}	+1.54^{I}	+1.78^{I}

[a] $E_{1/2}$ and $\triangle E$ in V. I = irreversible, hence value quoted is E_{pa}; QR = quasi-reversible; all other processes are reversible. Potentials for reversible processes are quoted from the cyclic voltammogram and potentials for quasi-reversible processes are quoted from the square wave voltammogram or the cyclic voltammogram. For quasi-reversible processes $\triangle E$ is only quoted where E_{pa} and E_{pc} are well defined. All potentials are vs. 0.01 mol L^{-1} $AgNO_3$/Ag. [b] Process overlaps with neighbouring process hence this is an estimated $E_{1/2}$ only. [c] As previously reported in reference.[9] [d] As previously reported in reference.[10] [e] When scanning out to −0.7 V an additional irreversible oxidation process is observed at +0.39 V which is associated with the reduction processes. [f] E_{pc} quoted (not $E_{1/2}$) since E_{pa} is poorly defined.

heme a_3 iron of cytochrome c oxidase and therefore seems less likely to bind exogenous ligands like oxygen, although the Cu^{I} ions will readily accept additional donor(s) on oxidation.

Electrochemical Studies on Mononuclear Cryptates

Unless otherwise stated, in this paper all potentials are quoted vs. 0.01 mol L^{-1} $AgNO_3$/Ag and all controlled potential experiments were carried out until the current reached 1% of the initial value.

The series of mononuclear cryptates show irreversible oxidation waves starting from about +1 V (Table 3) that are probably ligand-centred. In the case of iron(II) and cobalt(II), quasi-reversible oxidation waves at +0.78 and +0.29 V[9], respectively, which are likely to be attributable to metal-centred processes, are observed. For the copper(II) complex a reversible metal-centred reduction is observed at −0.38 V.[10]

The cyclic voltammogram of $[Mn^{II}L](ClO_4)_2$ (Figure 9, Table 3) reveals an irreversible oxidation process at +1.03 V. A coulometry experiment at +1.20 V resulted in no colour change and the transfer of 1.00 electron equivalents, indicating that this is a one-electron oxidation. Significant changes in the cyclic voltammogram of the complex after this oxidation indicated that this process is chemically irreversible. Further investigation would be required to determine whether the process at +1.03 V is metal- or ligand-centred. The absence of oxidation processes below +1.03 V indicates that the manganese(II) oxidation state is stabilised by the soft nitrogen donors and, more importantly, the seven coordinate geometry provided by L, as expected on the basis of the research of McKee and co-workers.[16] On scanning to negative potentials, three almost reversible, probably ligand-centred, processes are seen (Table 3). These are similar to the processes seen for $[Zn_2L](ClO_4)_4$ (see later), but are more spread out and occur at more negative potentials. Coulometry at −1.39 V resulted in the transfer of 1.80 electron equivalents and precipitation of the product. As all three reduction processes have similar peak heights and peak separations, it is likely that they are all two-electron processes. This provides further evidence that L is able to undergo two-electron reductions. However, it should be noted that the close proximity of these potentials diminishes confidence in the coulometric result.

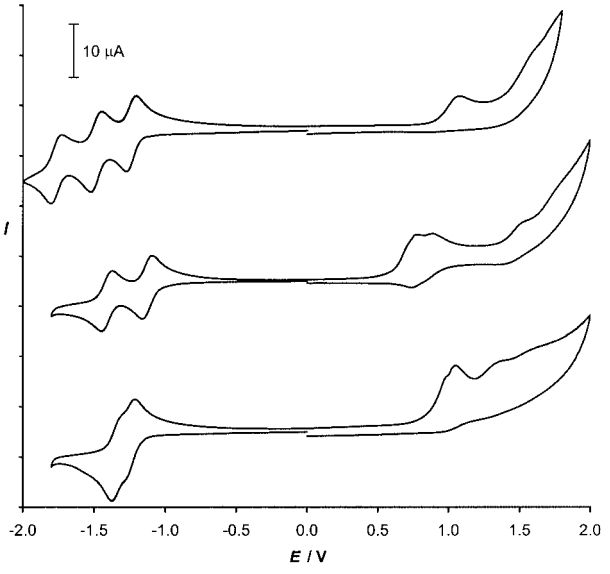

Figure 9. Full range cyclic voltammograms of the mononuclear cryptates $[Mn^{II}L](ClO_4)_2$ (top), $[Fe^{II}L](BF_4)_2$ (middle) and $[Ni^{II}L](BF_4)_2$ (bottom) in acetonitrile (200 mV s^{-1} vs. 0.01 mol L^{-1} $AgNO_3$/Ag); each scan starts at 0 V and initially scans to negative potentials

The cyclic voltammogram of the monoiron cryptate $[Fe^{II}L](BF_4)_2$ shows two almost reversible reductions (Figure 9, Table 3). A further quasi-reversible process is observed at −1.87 V (see Supporting Information). These processes are similar to the reduction processes observed for

$[Mn^{II}L](ClO_4)_2$, but start at slightly less negative potentials and are more spread out. Coulometry at −1.26 V resulted in the transfer of 1.89 electrons suggesting that they are two-electron processes. This reduction resulted in decomposition of the complex as indicated by the cyclic voltammograms recorded after the coulometry experiment. On scanning to positive potentials two closely overlapping quasi-reversible oxidation processes are observed. As noted earlier, at least one of these processes is likely to be due to Fe^{II} to Fe^{III} oxidation.

The cyclic voltammogram of the nickel cryptate $[Ni^{II}L](BF_4)_2$ shows two closely overlapping reversible reduction processes (Figure 9, Table 3). Coulometry at −1.50 V resulted in the transfer of 1.97 electron equivalents and some precipitation. This suggests that both processes correspond to one-electron transfers, assuming that precipitation occurred after the second process rather than after the first. On scanning to more negative potentials a further quasi-reversible reduction process occurs. On scanning to positive potentials two overlapping irreversible oxidation processes are seen (Table 3). Although we are unable, in the absence of ESR experiments, to decide unambiguously whether any processes in these cyclic voltammograms are metal-centred, the fact that no oxidation processes of any sort occur below +0.99 V in this case demonstrates the stability of the nickel(II) oxidation state in the cryptand.[17]

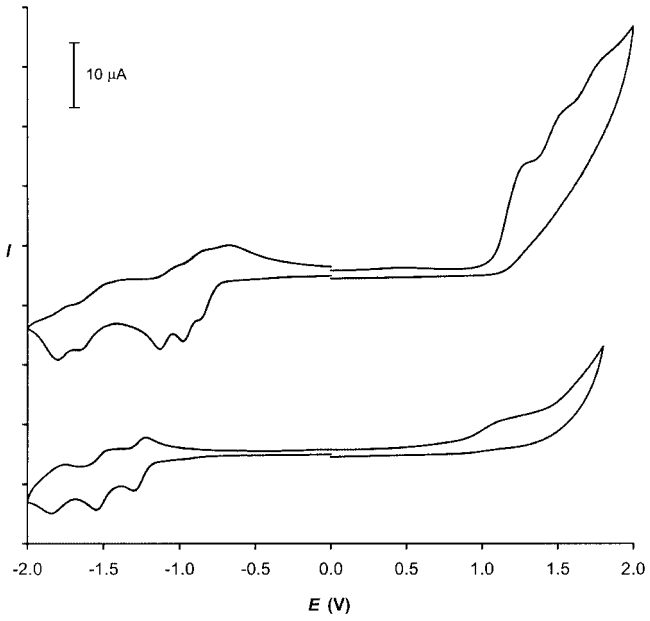

Figure 10. Full range cyclic voltammograms of $[Zn_2L](ClO_4)_4$ in acetonitrile before (top, two separate scans both starting from 0 V but one initially scanning to negative potentials and the other to positive potentials) and after (bottom, a single scan starting from 0 V and initially scanning to negative potentials) coulometry at −1.30 V (200 mV s^{-1} vs. 0.01 mol L^{-1} $AgNO_3$/Ag)

Electrochemical Studies on the Homodinuclear Zinc Cryptate

The electrochemistry of $[Zn_2L](ClO_4)_4$ was investigated in order to study the electrochemical processes of the L cryptand since the coordinated zinc ions are not expected to undergo reduction or oxidation in the potential range accessible in acetonitrile. The cyclic voltammogram of $[Zn_2L](ClO_4)_4$ shows three high-current irreversible oxidation processes as well as several reduction processes (Figure 10, Table 3). The oxidation processes had previously been observed in other cryptates of L,[10] and are also seen for some of the cryptates of L described here (Table 3), and are assigned to ligand oxidations. The first three overlapping reduction processes of $[Zn_2L](ClO_4)_4$ (Figure 11, Table 3) are almost reversible as indicated from a variable scan rate study. These processes are tentatively assigned to reduction of the three strands of the L cryptand. On scanning to more negative potentials two further quasi-reversible reduction processes are seen, which may correspond to further ligand reduction.

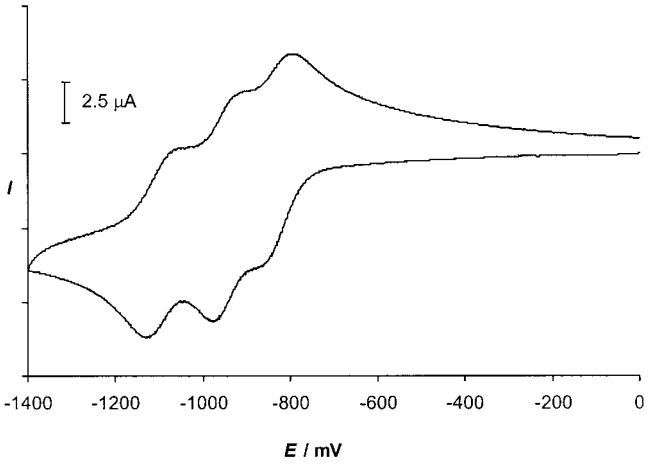

Figure 11. Cyclic voltammogram of $[Zn_2L](ClO_4)_4$ in acetonitrile showing the first three reversible reduction processes (200 mV s^{-1} vs. 0.01 mol L^{-1} $AgNO_3$/Ag). The scan starts at 0 V

The peak separations for the first two reduction processes in particular are smaller than expected for a one-electron process but larger than expected for a fully reversible two-electron process in our electrochemical cell. The closely overlapping nature of these processes made them difficult to study separately by coulometry. Coulometry at −1.30 V resulted in the transfer of just 2.00 electron equivalents, with coulometry at −1.05 V giving a similar result. During this two-electron reduction the pale yellow solution initially became an intense purple colour and then gradually became orange-yellow as the final two-electron reduction product formed. These colour changes could be accounted for by chemical reaction of an unstable radical product. Cyclic voltammograms measured after the two-electron reduction was complete demonstrate that the cryptate has indeed been altered: the behaviour at positive potentials has been affected (Figure 10), and whilst there are still three reduction processes at negative potentials, these are now at significantly more negative potentials and are more spread out (Figure 10 and 11). The processes, which now occur at $E_{1/2}$ = −1.26 V (ΔE = 0.07 V), −1.50 V (ΔE = 0.09 V) and −1.80 V (ΔE = 0.09 V), appear to be less reversible. These results indicate that the reduction of $[Zn_2L](ClO_4)_4$ is

chemically irreversible and that the product of this reduction is harder to reduce than the original complex.

Electrochemical Studies on Heterodinuclear Cryptates

The electrochemical properties of the series of heterodinuclear cryptates $[M^{II}Cu^{I}L](X)_3$ (M = Mn, Fe, Co, Ni; X = BF_4^- or ClO_4^-) were investigated to study the effect of the divalent cation on the electrochemistry of the copper(I) ion and vice versa. In all cases, following the addition of the Cu^{I} ion, a reversible or quasi-reversible wave corresponding to the $Cu^{I} \rightleftarrows Cu^{II}$ couple is observed in the voltammograms. This wave is usually in the potential range which is inactive in the monometallic precursor complexes (exceptions include the $[Co^{II}Cu^{I}L]^{3+}$ and $[Cu^{II}Cu^{I}L]^{3+}$ complexes). In addition, a copper deposition and stripping peak is observed following the application of potentials below about −1 V for all except the $[Fe^{II}Cu^{I}L]^{3+}$ complex.

The cyclic voltammogram of the heterodinuclear cryptate $[Mn^{II}Cu^{I}L](ClO_4)_2(BF_4)$ (Figure 12, Table 3) shares several features with that of $[Mn^{II}L](ClO_4)_2$, as well as additional features due to the presence of copper(I). The reduction region contains two almost reversible processes at $E_{1/2}$ = −1.25 V (ΔE = 0.08 V) and −1.46 V (ΔE = 0.09 V). These processes are similar to the first two reduction processes for $[Mn^{II}L](ClO_4)_2$ and are probably ligand-centred. On scanning to more negative potentials there are two further overlapping quasi-reversible processes with $E_{1/2}$ approximately equal to −1.77 and −1.89 V which are probably also ligand-centred. There is also an irreversible reduction process at −0.86 V. This process is associated with a stripping wave at −0.54 V (resulting from deposition of copper on the electrode), which is present when scanning to potentials below about −0.8 V, and is assigned to the $Cu^{I} \rightarrow Cu^{0}$ process.

There is an irreversible oxidation process at +1.07 V. This is similar to the process seen at +1.03 V for $[Mn^{II}L](ClO_4)_2$ and may be metal or ligand-centred. There is also an additional quasi-reversible oxidation process at $E_{1/2}$ = +0.25 V (ΔE = 0.10 V) and an irreversible oxidation process at about +0.81 V. Coulometry at +0.50 V resulted in the transfer of 1.06 electron equivalents leading to the assignment of the process at $E_{1/2}$ = +0.25 V to $Cu^{I} \rightleftarrows Cu^{II}$. The colour change from orange-brown to green during this oxidation is consistent with this assignment. The cyclic voltammogram of the bulk oxidation product was unchanged from that of the original $[Mn^{II}Cu^{I}L]^{3+}$ cyclic voltammogram, apart from some reduction in the peak size of the processes at +0.25 V and +1.07 V which may indicate partial decomposition of the complex.

The cyclic voltammogram of $[Fe^{II}Cu^{I}L](BF_4)_3{\cdot}CH_3CN$ shows three reversible reduction processes (Figure 12, Table 3). These are similar to the ligand-centred processes seen for $[Fe^{II}L](BF_4)_2$ although they occur at less negative potentials and are closer together. Coulometry at −1.15 V resulted in the transfer of 2.05 electron equivalents (I_f, 2.5% of I_i) and some precipitation. This suggests that the process at −1.07 V is a two-electron reduction. There is also an almost reversible oxidation process at $E_{1/2}$ = +0.49 V (ΔE = 0.10 V). Coulometry at +0.60 V resulted in the transfer of 1.40 electron equivalents (I_f, 2% of I_i). Although it is not possible to conclude whether this is a one- or two-electron process from coulometry, comparison with the cyclic voltammograms of $[M^{II}Cu^{I}L]^{3+}$ (M = Mn, Ni, Cu) indicates that this is probably a one-electron oxidation corresponding to $Cu^{I} \rightleftarrows Cu^{II}$. The cyclic voltammogram was largely unchanged after this oxidation, although all processes appeared less reversible and a small copper stripping wave was present at −0.56 V. This indicates that the complex was at least partially intact after oxidation. On scanning to more positive potentials two further irreversible oxidation processes are seen; one of these is likely to be due to oxidation of Fe^{II}.

The cyclic voltammogram of the heterodinuclear cryptate $[Ni^{II}Cu^{I}L](BF_4)_3{\cdot}H_2O$ is complex showing at least four closely spaced processes in the reduction region, with $E_{1/2}$

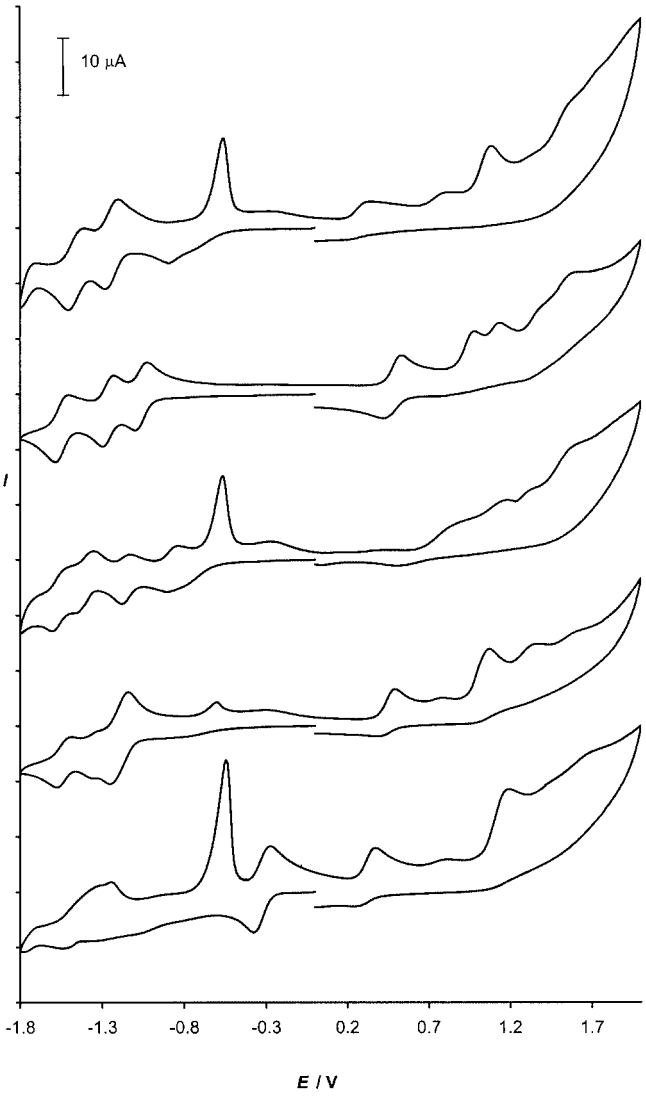

Figure 12. Full range cyclic voltammograms of the heterodinuclear cryptates in acetonitrile. From top to bottom: $[Mn^{II}Cu^{I}L](ClO_4)_2(BF_4)$, $[Fe^{II}Cu^{I}L](BF_4)_3{\cdot}CH_3CN$, $[Co^{II}Cu^{I}L](BF_4)_3$, $[Ni^{II}Cu^{I}L](BF_4)_3{\cdot}H_2O$ and $[Cu^{II}Cu^{I}L](BF_4)_3$ (200 mV s^{-1} vs. 0.01 mol L^{-1} $AgNO_3$/Ag); each scan starts at 0 V and initially scans to negative potentials

approximately equal to −1.19, −1.36, −1.53 and −1.89 V (Figure 12 and Supporting Information, Table 3). The overlapping nature of the processes meant that coulometry experiments could not be carried out. A small stripping wave occurs at −0.59 V when scanning to potentials below −1.00 V, which is due to the formation of copper on the electrode.

On scanning to positive potentials a reversible oxidation process is seen at $E_{1/2}$ = +0.46 V. Coulometry at +0.70 V resulted in the transfer of 1.01 electron equivalents indicating that this is a one-electron process. This process is therefore assigned to $Cu^{I} \rightleftarrows Cu^{II}$. Furthermore, the colour changed during this oxidation from orange-brown to green, consistent with this assignment. The cyclic voltammogram of the oxidation product was unchanged immediately after the oxidation, indicating that the $[Ni^{II}Cu^{II}L]^{4+}$ product is stable under argon in dry acetonitrile. The cyclic voltammogram of $[Ni^{II}Cu^{I}L](BF_4)_3{\cdot}H_2O$ also shows an irreversible oxidation process at +1.07 V, which may correspond to the oxidation of nickel(II) to nickel(III)[17] or a ligand-centred process.

As shown in Figure 12, the cyclic voltammogram of $[Co^{II}Cu^{I}L](BF_4)_3$ is complex with many processes (Table 3). The reduction region shows a series of quasi-reversible processes, as well as a stripping wave at −0.54 V. These processes are probably a mixture of metal- and ligand-centred reductions.

The oxidation region shows several quasi-reversible and irreversible processes. Applying a potential of 0.00 V failed to generate current flow confirming that oxidation occurs at positive potentials vs. $AgNO_3$/Ag(s). On scanning to positive potentials, there are two quasi-reversible processes with poorly resolved oxidation peaks on the forward scan and reduction peaks at +0.58 and +0.08 V on the return scan. Coulometry at +1.00 V resulted in the transfer of 2.00 electron equivalents and caused the colour of the complex to change from orange to dark brown. Subsequent coulometry at +0.25 V resulted in the transfer of 0.95 electron equivalents. These results suggest that the two quasi-reversible processes are both one-electron oxidations. As the Co^{II} to Co^{III} oxidation in the mononuclear cryptate $[Co^{II}L](BF_4)_2$ occurs at the relatively low potential of $E_{1/2}$ = +0.29 V,[9] it is possible that the cobalt(II) (rather than Cu^{I}) centre is oxidised first, followed by conformational changes deriving from the appreciably smaller radius of the Co^{III} cation.

The electrochemical properties of the heterodinuclear cryptates $[M^{II}Cu^{I}L](X)_3$ (M = Mn, Fe, Co, Ni, Cu, X = BF_4^- or ClO_4^-) indicate that the divalent cation influences the potential and reversibility of the $Cu^{I} \rightleftarrows Cu^{II}$ process (Table 3, Figure 13). For the cryptates $[M^{II}Cu^{I}L]^{3+}$ (M = Mn, Fe, Ni, Cu) the $E_{1/2}$ for the $Cu^{I} \rightleftarrows Cu^{II}$ process in CH_3CN is inversely correlated with the solid-state $M^{II}\cdots Cu^{I}$ distance and follows the order: Fe (+0.49 V; 4.72 Å) > Ni (+0.46 V; 4.86 Å) > Cu (+0.33 V; 4.96 Å) > Mn (+0.25 V; 5.23 Å). Therefore the influence of the divalent cation on the electrochemistry of the copper(I) ion is predominantly electrostatic, with the copper(I) ion becoming harder to oxidise with closer proximity to the positively charged divalent cation. The copper(I) ion appears to be most stable towards reduction and towards any subsequent dissociation in $[Fe^{II}Cu^{I}L](BF_4)_3{\cdot}CH_3CN$ since no stripping wave is observed, even on scanning to −1.80 V.

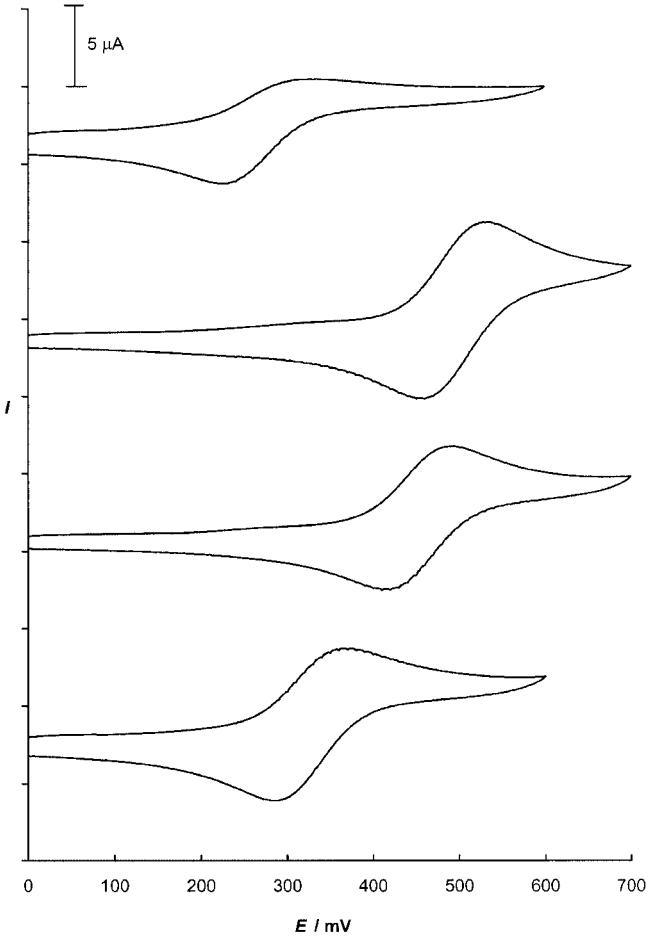

Figure 13. Cyclic voltammograms of heterodinuclear cryptates in acetonitrile showing the $Cu^{I} \rightleftarrows Cu^{II}$ process; from top to bottom: $[Mn^{II}Cu^{I}L](ClO_4)_2(BF_4)$, $[Fe^{II}Cu^{I}L](BF_4)_3{\cdot}CH_3CN$, $[Ni^{II}Cu^{I}L](BF_4)_3{\cdot}H_2O$ and $[Cu^{II}Cu^{I}L](BF_4)_3$ (200 mV s^{-1} vs. 0.01 mol L^{-1} $AgNO_3$/Ag); each scan starts at 0 V

Neither of the candidates for the $Cu^{I} \rightleftarrows Cu^{II}$ process for $[Co^{II}Cu^{I}L](BF_4)_3$, E_{pc} = +0.08 and +0.58 V ($M^{II}\cdots Cu^{I}$ 5.08 Å), fits into the above trend. This cryptate also shows the least reversible oxidation in this series of heterodinuclear cryptates. The anomalous behaviour of $[Co^{II}Cu^{I}L](BF_4)_3$ could be accounted for by the oxidation of the cobalt(II) ion (i.e. Co^{II} to Co^{III} at E_{pc} = +0.08 V) before the copper(I) ion (i.e. Cu^{I} to Cu^{II} at E_{pc} = +0.58 V). Oxidation of cobalt(II) to cobalt(III) may affect the M···Cu distance and would nevertheless enhance the positive charge (from +2 to +3) near the copper(I) ion, thus increasing its oxidation potential as observed.

It would be of interest to monitor the reciprocal effect of the copper(I) ion on the electrochemistry of the divalent cation in $[M^{II}Cu^{I}L](X)_3$ (M = Mn, Fe, Co, Ni, X = BF_4^- or ClO_4^-). However, this is ruled out due to the difficulty

of differentiating such metal-centred processes from ligand-centred processes with the facilities available to us.

Conclusion

The symmetrical cryptand L readily forms mononuclear cryptates with first-row transition-metal ions with geometries ranging from five to seven coordinate. Addition of copper(I) to these unsymmetrical monometallic cryptates results in the controlled formation of the heterodinuclear cryptates $[M^{II}Cu^{I}L](X)_3$ (M = Mn, Fe, Co, Ni, X = BF_4^- or ClO_4^-). This is the first series of this kind to be reported.

The syntheses of $[Zn_2L](ClO_4)_4$ and $Mn_2LCl_4{\cdot}H_2O$ demonstrate that L can also form homodinuclear complexes with relatively non-stereochemically demanding divalent cations. However, the choice of counterion and/or solvent appears to be crucial for the formation of the dinuclear complexes, and there is evidence of interaction of the counterions with the divalent zinc or manganese ions. Electrochemical studies on $[Zn_2L](ClO_4)_4$ revealed that the L cryptand is able to undergo a series of reductions and oxidations, which were also observed in several other cryptates of L.

The series of heterodinuclear cryptates has been structurally characterised. In all cases, the divalent cation has a distorted octahedral geometry and the copper(I) ion has a distorted trigonal pyramidal geometry. The $M^{II}\cdots Cu^{I}$ distance in these cryptates decreases with decreasing ionic radius of the divalent cation.

Cyclic voltammetric studies on this series of heterodinuclear cryptates show that the $E_{1/2}$ of the Cu^{I}/Cu^{II} couple follows the order Fe > Ni > Cu > Mn and is inversely correlated to the $M^{II}\cdots Cu^{I}$ distance. The previously synthesised $[Co^{II}Cu^{I}L](BF_4)_3$ does not follow this trend, probably because the cobalt ion is in the +3 state at the time when Cu^{I} is oxidised.

Experimental Section

General: 3,6-Diformylpyridazine,[18] L[9] and $Cu^{I}(MeCN)_4X$ (X = BF_4^-)[19] were synthesised as described previously. For the electrochemical studies HPLC grade MeCN was distilled from CaH_2 immediately before use. Chloroform was extracted with the equivalent volume of water, four times, and dried over Na_2SO_4, before use. All other solvents and reagents were used as received. Physical measurements were carried out as described previously,[18,20] except for the following: the electrochemistry was carried out with 1 mmol L^{-1} dry acetonitrile solutions and 0.1 mol L^{-1} tetraethylammonium perchlorate or tetrabutylammonium hexafluorophosphate as the supporting electrolyte, on an EG&G Princeton Applied Research 273A potentiostat using a 0.01 mol L^{-1} $AgNO_3$/Ag reference electrode. As a further reference check, ferrocene was added at the conclusion of each experiment: the Fc/Fc^+ couple consistently occurred at $E_{1/2}$ = +0.07 ± 0.01 V with ΔE = 0.07 V. Magnetic measurements were carried using a Johnson−Matthey magnetic susceptibility balance MSB-MKI. All magnetic data were corrected for diamagnetic contributions using Pascal's constants.

Caution: *Whilst no problems were encountered in the course of this work perchlorate mixtures are potentially explosive and should therefore be handled with appropriate care.*

Preparation of $[Mn^{II}L](ClO_4)_2$: L (0.060 g, 0.1 mmol) was suspended in methanol (20 mL) and stirred. To this was added a methanol solution (10 mL) of $Mn(ClO_4)_2{\cdot}6H_2O$ (0.037 g, 0.1 mmol) which caused the cream suspension to turn bright yellow. After stirring overnight, the suspension was filtered yielding $[Mn^{II}L](ClO_4)_2$ as a yellow powder (0.066 g, 77%). Single crystals suitable for X-ray diffraction were obtained by recrystallisation of the product from DMF by vapour diffusion of diethyl ether. IR (KBr, inter alia): $\tilde{\nu}$ = 3415 (b, s), 1652 (m), 1144 (s), 1116 (s), 1088 (s), 625 cm^{-1} (m). UV/Vis (MeCN): λ_{max} (ε) = 208 (62100), 250 nm (35100 L $mol^{-1}cm^{-1}$), 290 (sh). MS (ESI): *m/z* (%) = 746 (34) $[MnC_{30}H_{36}N_{14}(ClO_4)^+]$, 324 (100) $[MnC_{30}H_{36}N_{14}^{2+}]$. μ = 6.3 BM (293 K); Λ_m(MeCN) = 280 $mol^{-1}\,cm^2\,\Omega^{-1}$ (2:1 = 220−300 $mol^{-1}\,cm^2\,\Omega^{-1}$).[12] $C_{30}H_{36}MnN_{14}(ClO_4)_2$ (846.6): calcd. C 42.56, H 4.29, N 23.16; found C 42.44, H 4.47, N 22.97.

Preparation of $[Fe^{II}L](BF_4)_2$: L (0.045 g, 0.08 mmol) was suspended in degassed acetonitrile (30 mL) and stirred under a nitrogen atmosphere. To this was added an acetonitrile solution (5 mL) of $Fe(BF_4)_2{\cdot}6H_2O$ (0.026 g, 0.08 mmol), which caused the suspension to clarify and become deep purple. After stirring under a nitrogen atmosphere for 4 h the volume of the solution was reduced to about 15 mL in vacuo. Diethyl ether diffusion into the resulting solution gave $[Fe^{II}L](BF_4)_2$ as a purple crystalline solid (0.032 g, 52%). ^1H NMR (500 MHz, solvent CD_3CN, reference CH_3CN, 243 K): δ = 8.94 (s, 1 H, H^{11}), 8.24 (d, 1 H, H^3), 8.08 (d, 1 H, H^4), 7.37 (s, 1 H, H^6), 3.71−3.88 (m, 3 H, H^{7b}, H^{10a}, H^{10b}), 3.61 (br, d, 1 H, H^{9b}), 3.39 (br, t, 1 H, H^{9a}), 3.30 (t, 1 H, H^{7a}), 2.95 (t, 1 H, H^{8a}), 2.36 (m, 1 H, H^{8b}); at 298 K: 8.49 (s, br), 8.16 (d), 7.48 (s), 3.94 (s, br), 3.82 (dt), 3.59 (s, br), 3.37 (t), 3.00 (t), 2.40 (dd). IR (KBr, inter alia): $\tilde{\nu}$ = 3414 (b, s), 1638 (m), 1617 (m), 1534 (w), 1437 (m), 1053 (s), 1032 (s), 521 cm^{-1} (w). UV/Vis (MeCN): λ_{max} (ε) = 213 (64700), 250 (sh), 370 (sh), 428 (4800), 540 (sh), 588 nm (8030 L $mol^{-1}\,cm^{-1}$). MS (ESI): *m/z* (%) = 735 (26) $[FeC_{30}H_{36}N_{14}(BF_4)^+]$, 648 (25) $[FeC_{30}H_{36}N_{14}^+]$, 615 (100) $[NaC_{30}H_{36}N_{14}^+]$, 324 (69) $[FeC_{30}H_{36}N_{14}^{2+}]$. Λ_m(MeCN) = 286 $mol^{-1}\,cm^2\,\Omega^{-1}$ (2:1 = 220−300 $mol^{-1}\,cm^2\,\Omega^{-1}$).[12] $C_{30}H_{36}FeN_{14}(BF_4)_2$ (822.2): calcd. C 43.83, H 4.41, N 23.85; found C 43.78, H 4.54, N 23.86.

Preparation of $[Ni^{II}L](BF_4)_2$: L (0.062 g, 0.1 mmol) was suspended in acetonitrile (40 mL) and stirred. To this was added an acetonitrile solution (10 mL) of $Ni(BF_4)_2{\cdot}6H_2O$ (0.036 g, 0.1 mmol), which caused the suspension to clarify and become pale greenish yellow. After stirring overnight, the volume was reduced to about 10 mL in vacuo. Diffusion of diethyl ether into the resulting solution gave brown crystals of $[Ni^{II}L](BF_4)_2$ (0.069 g, 80%). IR (KBr, inter alia): $\tilde{\nu}$ = 3419 (b, s), 1647 (m), 1440 (m), 1050 (s), 521 cm^{-1} (w). UV/Vis (MeCN): λ_{max} (ε) = 211 (68700), 250 (sh), 825 (30), 908 nm (30 L $mol^{-1}\,cm^{-1}$). MS (ESI): *m/z* (%) = 737 (52) $[NiC_{30}H_{36}N_{14}(BF_4)^+]$, 325 (100) $[NiC_{30}H_{36}N_{14}^{2+}]$. μ = 3.1 BM (293 K); Λ_m(MeCN) = 301 $mol^{-1}\,cm^2\,\Omega^{-1}$ (2:1 = 220−300 $mol^{-1}\,cm^2\,\Omega^{-1}$).[12] $C_{30}H_{36}N_{14}Ni(BF_4)_2$ (825.0): calcd. C 43.67, H 4.40, N 23.77; found C 43.86, H 4.42, N 23.57.

Preparation of $[Ni^{II}L](ClO_4)_2$: L (0.029 g, 0.05 mmol) was suspended in acetonitrile (10 mL) and stirred. To this was added an acetonitrile solution (8 mL) of $Ni(ClO_4)_2{\cdot}6H_2O$ (0.018 g, 0.05 mmol), which caused the suspension to clarify and become pale greenish yellow. After stirring overnight, the volume was reduced to about 5 mL in vacuo. Diffusion of diethyl ether into the

resulting solution gave brown crystals of $[Ni^{II}L](ClO_4)_2$ (0.034 g, 81%). IR (KBr, inter alia): $\tilde{\nu}$ = 3414 (b, m), 2916 (m), 2849 (m), 1647 (m), 1442 (m), 1329 (m), 1083 (b, s), 622 cm^{-1} (s). $C_{30}H_{36}N_{14}Ni(ClO_4)_2$ (850.3): calcd. C 42.38, H 4.27, N 23.06; found C 42.55, H 4.18, N 23.19.

Preparation of $[Zn_2L](ClO_4)_4$: L (0.120 g, 0.2 mmol) was suspended in acetonitrile (50 mL) and stirred. To this was added an acetonitrile solution (5 mL) of $Zn(ClO_4)_2{\cdot}6H_2O$ (0.151 g, 0.4 mmol), which caused the cream suspension to clarify and become bright yellow. After stirring overnight, the volume was reduced to about 20 mL in vacuo. Diffusion of diethyl ether into the resulting solution gave $[Zn_2L](ClO_4)_4$ as a yellow crystalline solid (0.181 g, 80%). ^1H NMR (500 MHz, solvent CD_3CN, reference CH_3CN, 298 K): δ = 8.96 (s, 1 H, H^6), 8.34 (s, 1 H, H^3), 3.97 (br, t, 1 H, H^{7a}), 3.77 (dd, 1 H, H^{7b}), 3.24 (dd, 1 H, H^{8b}), 3.08 (td, 1 H, H^{8a}). ^{13}C NMR (126 MHz, solvent CD_3CN, reference CH_3CN, 298 K): δ = 166.1 (C^6), 153.7 (C^2), 135.1 (C^3), 58.8 (C^7), 54.0 (C^8). IR (KBr, inter alia): $\tilde{\nu}$ = 3417 (s, b), 1653 (m), 1437 (w), 1326 (w), 1147 (s), 1121 (s), 1077 (s), 637 (m), 629 (m), 624 cm^{-1} (m). UV/Vis (MeCN): λ_{max} (ε) = 206 (51900), 251 (30400 L mol^{-1} cm^{-1}), 290 (sh), 350 (sh) nm. MS (ESI): *m/z* (%) = 757 (73) $[ZnC_{30}H_{36}N_{14}(ClO_4)^+]$, 328 (100) $[ZnC_{30}H_{36}N_{14}{}^{2+}]$. Λ_m(MeCN) = 359 mol^{-1} cm^2 Ω^{-1} (3:1 = 340−420 mol^{-1} cm^2 Ω^{-1}).[12] $C_{30}H_{36}N_{14}Zn_2(ClO_4)_4$ (1121.3): calcd. C 32.13, H 3.24, N 17.49; found C 32.09, H 3.46, N 17.33. NMR spectroscopic data for the mononuclear zinc(II) complex $[ZnL](ClO_4)_2$: ^1H NMR (500 MHz, solvent CD_3CN, reference CH_3CN, 298 K): δ = 8.93 (d, 1 H, H^{11}), 8.35 (d, 1 H, H^3), 8.11 (d, 1 H, H^4), 7.38 (d, 1 H, H^6), 4.23 (tdd, 1 H, H^{10b}), 3.88 (dd, 1 H, H^{10a}), 3.83 (m, 1 H, H^{7b}), 3.32 (t, 1 H, H^{7a}), 3.17−3.29 (m, 2 H, H^{9a}, H^{9b}), 2.98 (td, 1 H, H^{8a}), 2.52 (dd, 1 H, H^{8b}). ^{13}C NMR (126 MHz, solvent CD_3CN, reference CH_3CN, 298 K): δ = 163.0 (C^{11}), 160.2 (C^5), 159.6 (C^6), 152.3 (C^2), 131.9 (C^4), 128.2 (C^3), 60.6 (C^7), 56.0 (C^1), 55.3 (C^8), 53.2 (C^9).

Preparation of $Mn^{II}_2LCl_4{\cdot}H_2O$: L (0.060 g, 0.10 mmol) was suspended in methanol (25 mL) and stirred. To this was added a methanol solution (5 mL) of $MnCl_2{\cdot}4H_2O$ (0.040 g, 0.20 mmol), which caused the cream suspension to turn bright yellow and clarify. After stirring overnight, the volume was reduced to about 10 mL in vacuo. Diffusion of diethyl ether into the resulting solution gave $Mn_2LCl_4.H_2O$ as a yellow crystalline solid (0.075 g, 88%). IR (KBr, inter alia): $\tilde{\nu}$ = 3445 (b, s), 1651 (s), 1433 (m), 1326 (m), 1035 (m), 927 (m), 581 cm^{-1} (w). UV/Vis (MeOH): λ_{max} (ε) = 250 nm (36300 L mol^{-1} cm^{-1}). MS (ESI): *m/z* (%) = 324 (100) $[MnC_{30}H_{36}N_{14}{}^{2+}]$, 216 (29) $[MnC_{30}H_{36}N_{14}H^{3+}]$. μ = 6.1 BM per Mn (293 K); Λ_m(MeOH) = 224 mol^{-1} cm^2 Ω^{-1} (2:1 = 160−220 mol^{-1} cm^2 Ω^{-1}).[12] $C_{30}H_{36}N_{14}Mn_2Cl_4{\cdot}H_2O$ (862.4): calcd. C 41.78, H 4.44, N 22.74, Cl 16.44; found C 42.79, H 4.13, N 22.46, Cl 16.44.

Preparation of $[Na_2L](CF_3SO_3)_2$: L (0.040 g, 0.07 mmol) was suspended in acetonitrile (20 mL) and stirred. To this was added an acetonitrile solution (10 mL) of $Na(CF_3SO_3)$ (0.024 g, 0.14 mmol), which caused the suspension to clarify slightly. After stirring overnight, the mixture was filtered to remove unreacted L. Diffusion of diethyl ether into the resulting solution gave the product as a white crystalline solid (0.021 g, 33% yield). ^1H NMR (500 MHz, solvent CD_3CN, reference CH_3CN, 298 K): δ = 8.56 (s, 1 H, H^6), 7.96 (s, 1 H, H^3), 3.86 (t, 2 H, H^7), 2.95 (t, 2 H, H^8). ^{13}C NMR (126 MHz, solvent CD_3CN, reference CH_3CN, 298 K): δ = 160.2 (C^6), 156.2 (C^2), 131.7 (C^3), 58.7 (C^7), 54.7 (C^8). IR (KBr, inter alia): $\tilde{\nu}$ = 3414 (m, b), 2850 (m), 2806 (m), 1654 (m), 1266 (s), 1223 (m), 1146 (s), 1033 (s), 639 (s), 516 cm^{-1} (m). UV/Vis (MeCN): λ_{max} (ε) = 247 nm (50400 L mol^{-1} cm^{-1}). MS (ESI): *m/z* (%) = 615 (100) $[NaC_{30}H_{36}N_{14}{}^+]$. $C_{30}H_{36}N_{14}Na_2(CF_3SO_3)_2$ (936.8): calcd. C 41.03, H 3.87, N 20.93; found C 41.07, H 3.95, N 21.09.

Preparation of $[M^{II}Cu^{I}L](X)_3$ (M = Mn, Fe, Ni, X = BF_4^- or ClO_4^-): L (0.06 g, 0.1 mmol) was suspended in acetonitrile (40 mL) and stirred under a nitrogen atmosphere. To this was added an acetonitrile solution (10 mL) of an appropriate salt of the divalent cation (0.1 mmol), which caused the suspension to clarify. After stirring for 30 min, solid $Cu^I(CH_3CN)_4BF_4$ (0.03 g, 0.1 mmol) was added to the solution causing it to change colour. After stirring overnight, the volume was reduced to about 20 mL in vacuo. Diffusion of diethyl ether into the resulting solution gave the products as crystalline solids.

$[Mn^{II}Cu^{I}L](ClO_4)_2(BF_4)$: Prepared as above, except that $Cu^I(CH_3CN)_4BF_4$ (0.035 g, 0.11 mmol) was added. Reddish brown crystals (0.088 g, 88% yield). IR (KBr, inter alia): $\tilde{\nu}$ = 3482 (b, s), 1652 (m), 1575 (w), 1440 (w), 1325 (w), 1143 (s), 1117 (s), 1083 (s), 1032 (m), 628 cm^{-1} (m). UV/Vis (MeCN): λ_{max} (ε) = 250 nm (33000 L mol^{-1} cm^{-1}), 280 (sh). MS (FAB): *m/z* (%) = 910 (17) $[MnCuC_{30}H_{36}N_{14}(ClO_4)_2]$, 809 (100) $[MnCuC_{30}H_{36}N_{14}(ClO_4)]$, 797 (26) $[MnCuC_{30}H_{36}N_{14}(BF_4)]$, 710 (48) $[MnCuC_{30}H_{36}N_{14}]$, 655 (77) $[CuC_{30}H_{36}N_{14}]$. μ = 5.9 BM (293 K); Λ_m(MeCN) = 407 $mol^{-1}cm^2\Omega^{-1}$ (3:1 = 340−420 mol^{-1} cm^2 Ω^{-1}).[12] $C_{30}H_{36}CuMnN_{14}(ClO_4)_2(BF_4)$ (996.9): calcd. C 36.15, H 3.64, N 19.67, Mn 5.51, Cu 6.37; found C 36.15, H 3.61, N 19.52, Mn 5.27, Cu 6.11.

$[Fe^{II}Cu^{I}L](BF_4)_3{\cdot}CH_3CN$: Prepared as above, except that the crude product was precipitated out by the addition of diethyl ether (approximately 50 mL) and then recrystallised from acetonitrile to give purple crystals (0.076 g, 75% yield). ^1H NMR (500 MHz, solvent CD_3CN, reference CH_3CN, 298 K): δ = 9.03 (s, 1 H, H^{11}), 8.56 (d, 1 H, H^6), 8.33 (d, 1 H, H^3), 7.90 (d, 1 H, H^4), 3.67 (dd, 1 H, H^{10b}), 3.62 (ddd, 1 H, H^{7a}), 3.54 (dd, 1 H, H^{7b}), 3.45−3.52 (m, 2 H, H^{10a}, H^{9b}), 3.25 (m, 1 H, H^{9a}), 3.08 (dd, 1 H, H^{8b}), 2.91 (td, 1 H, H^{8a}). ^{13}C NMR (126 MHz, solvent CD_3CN, reference CH_3CN, 298 K): δ = 170.8 (C^{11}), 161.6 (C^2), 158.9 (C^6), 157.5 (C^5), 131.6 (C^3), 128.1 (C^4), 61.1 (C^7), 60.6 (C^1), 54.6 (C^9), 52.3 (C^8). IR (KBr, inter alia): $\tilde{\nu}$ = 3424 (br), 1635 (m), 1532 (m), 1312 (m), 1123 (s), 1083 (s), 1034 (s), 533 (w), 521 cm^{-1} (w). UV/Vis (MeCN): λ_{max} (ε) = 211 (75000), 390 (sh), 441 (10700), 540 (sh), 580 nm (10500 L mol^{-1} cm^{-1}). MS (FAB): *m/z* (%) = 711 (100) $[FeCuC_{30}H_{36}N_{14}]$, 648 (86) $[FeC_{30}H_{36}N_{14}]$. μ = 0.0 BM (293 K); Λ_m(MeCN) = 393 mol^{-1} cm^2 Ω^{-1} (3:1 = 340−420 mol^{-1} cm^2 Ω^{-1}).[12] $C_{30}H_{36}CuFeN_{14}(BF_4)_3.CH_3CN$ (1013.6): calcd. C 37.92, H 3.88, N 20.73, Fe 5.51, Cu 6.27; found C 37.97, H 3.95, N 20.57, Fe 5.28, Cu 6.74.

$[Ni^{II}Cu^{I}L](BF_4)_3{\cdot}2H_2O$: Reddish brown crystals (0.076 g, 75% yield). IR (KBr, inter alia): $\tilde{\nu}$ = 3419 (b), 1636 (m), 1083 (s), 1035 (s), 533 (w), 521 cm^{-1} (w). UV/Vis (MeCN): λ_{max} (ε) = 250 (sh), 413 (2560), 806 nm (20 L mol^{-1} cm^{-1}). MS (ESI): *m/z* (%) = 737 (7) $[NiC_{30}H_{36}N_{14}BF_4{}^+]$, 400 (2) $[NiCuC_{30}H_{36}N_{14}BF_4{}^{2+}]$, 325 (100) $[NiC_{30}H_{36}N_{14}{}^{2+}]$, 238 (33) $[NiCuC_{30}H_{36}N_{14}{}^{3+}]$. μ = 3.1 BM (293 K); Λ_m(MeCN) = 410 mol^{-1} cm^2 Ω^{-1} (1:3 = 340−420 mol^{-1} cm^2 Ω^{-1}).[12] $C_{30}H_{36}CuNiN_{14}(BF_4)_3{\cdot}2H_2O$ (1011.4): calcd. C 35.63, H 3.99, N 19.39, Ni 5.80, Cu 6.28; found C 36.00, H 3.67, N 19.16, Ni 5.62, Cu 6.25.

X-ray Crystallography: Data were collected on Bruker SMART diffractometers (Universities of Canterbury, Auckland and Bristol), using graphite-monochromated Mo-K_α radiation (λ = 0.71013 Å). The data were corrected for Lorentz and polarisation effects and semi-empirical absorption corrections were applied. The structures were solved by direct methods (SHELXS-97)[21] and refined against all F^2 data. (SHELXL-97).[22] Hydrogen atoms were inserted at cal-

Table 4. Crystallographic data for mononuclear and heterodinuclear cryptates of L

	$[Mn^{II}L](ClO_4)_2$	$[Ni^{II}L](ClO_4)_2$	$[Mn^{II}Cu^{I}L](ClO_4)_2(BF_4)$	$[Fe^{II}Cu^{I}L](BF_4)_3{\cdot}2.5CH_3CN$	$[Ni^{II}Cu^{I}L](BF_4)_3$
Formula	$C_{30}H_{36}Cl_2MnN_{14}O_8$	$C_{30}H_{36}Cl_2N_{14}NiO_8$	$C_{30}H_{36}CuMnN_{14}$[a]	$C_{35}H_{43.5}B_3CuF_{12}FeN_{16.5}$	$C_{30}H_{36}B_3CuF_{12}N_{14}NiO_{0.5}$
M_r	846.57	850.34	711.21[a]	1075.18	983.41
T [K]	173(2)	168(2)	168(2)	150(2)	150(2)
Crystal system	triclinic	triclinic	monoclinic	triclinic	triclinic
Space group	$P\bar{1}$	$P\bar{1}$	$P2_1/n$	$P\bar{1}$	$P\bar{1}$
a [Å]	9.6480(15)	9.738(4)	14.552(5)	9.84300(10)	12.67870(10)
b [Å]	13.316(3)	13.455(5)	15.406(5)	12.2499(2)	16.46700(10)
c [Å]	29.505(7)	29.674(11)	19.100(6)	20.03170(10)	21.2814(2)
α [°]	84.158(17)°	82.310(5)	90	82.4530(10)	96.1030(10)
β [°]	87.220(13)°	86.256(4)	110.982(4)	78.1380(10)	90.7510(10)
γ [°]	75.811(15)°	73.277(4)	90	74.1800(10)	90.5490(10)
V [Å^3]	3654.7(13)	3689(2)	3998(2)	2266.94(5)	4417.30(6)
Z	4	4	4	2	4
$\rho_{calcd.}$ [g/cm^3]	1.539	1.531	1.182[a]	1.575	1.479
μ [mm^{-1}]	0.578	0.740	0.885[a]	0.888	1.000
F(000)	1748	1760	1472[a]	1094	1992
Crystal size [mm]	0.50 × 0.50 × 0.49	0.61 × 0.56 × 0.40	0.55 × 0.45 × 0.07	0.28 × 0.18 × 0.08	0.48 × 0.40 × 0.24
θ range for data collection [°]	1.58 to 27.48	2.08 to 26.36	2.19 to 25.35	1.04 to 25.39	2.57 to 25.84
Reflections collected	38185	44887	46991	20354	40919
Independent reflections	16565	14572	7322	8270	16742
R(int)	0.0357	0.0381	0.0440	0.0267	0.0208
Max. and min. transmission	0.86 and 0.61	0.76 and 0.66	1.00 and 0.88	0.95 and 0.85	0.84 and 0.71
Data /parameters	16565/ 991	14572/991	7322/990	8270/660	16742/1206
Goof (F^2)	1.102	1.174	1.089	1.041	1.030
R_1 [$I > 2\sigma(I)$]	0.0540	0.0867	0.0499	0.0512	0.0506
wR_2 [all data]	0.1566	0.2052	0.1364	0.1387	0.1249

[a] Due to the use of SQUEEZE[23] these values refer only to the disordered cation.

culated positions (except where noted) and rode on the atoms to which they are attached (including isotropic thermal parameters which were equal to 1.2 times the equivalent isotropic displacement parameter for the attached non-hydrogen atom) and all non-hydrogen atoms were made anisotropic. CCDC 224698−224703 contain the supplementary crystallographic data for this paper. These data can be obtained free of charge via www.ccdc.cam.ac.uk/conts/retrieving.html [or from the Cambridge Crystallographic Data Centre, 12 Union Road, Cambridge CB2 1EZ, UK; Fax: (internat.) + 44-1223-336-033; E-mail: deposit@ccdc.cam.uk].

$[Mn^{II}Cu^{I}L_I](ClO_4)_2(BF_4)$: Notwithstanding several 0k0 reflections for which $I/\sigma(I) > 5$, we have solved this structure in $P2_1/n$. In space group Pn the pairs of cations are very clearly related by a centre of symmetry. The appearance of significant intensity for the 0k0 reflections is attributed to partial ordering of the anion species: in space group $P2_1/n$, each of the three anion sites is a composite of BF_4^- and ClO_4^- and in space group Pn ordering of the anions was not discernible. In view of the highly disordered anion sites, which together indicated an approximately 2:1 ratio ClO_4^-:BF_4^-, the structure was subjected to the SQUEEZE procedure of the PLATON suite.[23] A void volume of 968 Å^3 per cell containing 562 electrons was calculated. The electron count is very close to that calculated (568 electrons) for 8ClO_4^- and 4BF_4^- per cell. In contrast to poor convergence behaviour for refinements with disordered anion species, refinements on the SQUEEZEd structure converged quickly.

$[Fe^{II}Cu^{I}L_I](BF_4)_3{\cdot}2.5CH_3CN$: One of the BF_4^- anions was disordered over two sites with a common fluorine atom. One of the two acetonitrile molecules was disordered across a centre of inversion.

$[Ni^{II}Cu^{I}L_I](BF_4)_3$: The two complete cryptates in the asymmetric unit were both "end-for-end" disordered: in the first cryptate Cu(1) and Ni(2) are 0.76 occupancy [Cu(2) and Ni(1) minor occupancy] and in the second cryptate Cu(4) and Ni(3) are 0.65 occupancy [Cu(3) and Ni(4) minor occupancy]. Consequently the pyridazine rings of all strands are also disordered and this has been modelled. The SQUEEZE option of PLATON[23] was used to account better for the disordered anions and solvent molecules. This was found to be a reasonable approach as a total of 740 electrons in the void volume per cell was calculated, slightly greater than that of the best model, which comprised twelve BF_4^-, eight CH_3CN and four H_2O species for a total of 720 electrons per cell.

For crystal data see Table 4.

Supporting Information (see also footnote on the first page of this article): A table of the UV/Vis spectroscopic data, the ^{1}H NMR spectrum of $[ZnL](ClO_4)_2$, a summary of the X-ray structural parameters for $[Fe^{II}L](BF_4)_2$, and additional cyclic voltammograms of the cryptates described in this paper are provided.

Acknowledgments

This work was supported by grants from the University of Otago. We are grateful to Dr. J. Wikaira and Professor W. T. Robinson (University of Canterbury), and T. Groutso and Professors C. E. F. Rickard and P. D. W. Boyd (University of Auckland) for the X-ray data collections. We acknowledge the EPSRC Swansea FAB mass spectrometry service (Swansea) and B. M. Clark (University of Canterbury) for the mass spectra, Simon S. Iremonger (University of Otago) for re-running the UV/Vis spectrum of the dizinc(II) cryptate and a referee for helpful comments. SB thanks the Univer-

sity of Otago for the granting of study leave and gratefully acknowledges her hosts Professor J. Nelson and the financial support of a Queens University Belfast Visiting Professorship and subsequently her hosts Dr. J. C. Jeffery, Professors M. D. Ward and J. McCleverty and the financial support of a Royal Society of Chemistry Journals Grant.

[1] J. Nelson, V. McKee, G. Morgan, *Prog. Inorg. Chem.* **1998**, *47*, 167−317.
[2] V. McKee, *Adv. Inorg. Chem.* **1993**, *40*, 323−399.
[3] O. Kahn, *Struct. Bond.* **1987**, *68*, 89−167.
[4] F. Avecilla, C. Platas-Iglesias, R. Rodríguez-Cortiñas, G. Guillemot, J.-C. G. Bünzli, C. D. Brondino, C. F. G. C. Geraldes, A. d. Blas, T. Rodríguez-Blas, *J. Chem. Soc., Dalton Trans.* **2002**, 4658−4665; R. Rodríguez-Cortiñas, F. Avecilla, C. Platas-Iglesias, D. Imbert, J.-C. G. Bünzli, A. de Blas, T. Rodríguez-Blas, *Inorg. Chem.* **2002**, *41*, 5336−5349; Q.-Y. Chen, Q.-H. Luo, Z.-L. Wang, J.-T. Chen, *Chem. Commun.* **2000**, 1033−1034; Q.-Y. Chen, Q.-H. Luo, D.-J. Fu, J.-T. Chen, *J. Chem. Soc., Dalton Trans.* **2002**, 2873−2878; Q.-Y. Chen, Q.-H. Luo, L.-M. Zheng, Z.-L. Wang, J.-T. Chen, *Inorg. Chem.* **2002**, *41*, 605−609; Q.-Y. Chen, Q.-H. Luo, X.-L. Hu, M.-C. Shen, J.-T. Chen, *Chem. Eur. J.* **2002**, *8*, 3984−3990.
[5] M. D. Timken, W. A. Marritt, D. N. Hendrickson, R. A. Gagné, E. Sinn, *Inorg. Chem.* **1985**, *24*, 4202−4208.
[6] R. E. Marsh, W. P. Schaefer, *Inorg. Chem.* **1986**, *25*, 3661−3662.
[7] J.-L. Pierre, P. Chantemps, S. M. Refaif, C. G. Beguin, A. El-Marzouki, G. Serratrice, P. Rey, J. Langier, *J. Chem. Soc., Chem. Commun.* **1994**, 1117−1118; J.-L. Pierre, P. Chantemps, S. M. Refaif, C. G. Beguin, A. El-Marzouki, G. Serratrice, E. Saint-Aman, P. Rey, *J. Am. Chem. Soc.* **1995**, *117*, 1965−1973.
[8] S. Brooker, J. D. Ewing, J. Nelson, J. C. Jeffery, *Inorg. Chim. Acta* **2002**, *337*, 463−466.
[9] S. Brooker, J. D. Ewing, J. Nelson, *Inorg. Chim. Acta* **2001**, *317*, 53−58.
[10] S. Brooker, J. D. Ewing, T. K. Ronson, C. J. Harding, J. Nelson, D. J. Speed, *Inorg. Chem.* **2003**, *42*, 2764−2773.
[11] S. Cromie, F. Launay, V. McKee, *Chem. Commun.* **2001**, 1918−1919.
[12] W. J. Geary, *Coord. Chem. Rev.* **1971**, *7*, 81−122.
[13] Q. Lu, J. M. Latour, C. J. Harding, N. Martin, D. J. Marrs, V. McKee, J. Nelson, *J. Chem. Soc., Dalton Trans.* **1994**, 1471−1478; D. J. Marrs, V. McKee, J. Nelson, Q. Lu, C. J. Harding, *Inorg. Chim. Acta* **1993**, *211*, 195−202.
[14] F. A. Cotton, G. Wilkinson, C. A. Murillo, M. Bochmann, *Advanced Inorganic Chemistry*, 6th ed., John Wiley & Sons, Inc., New York, **1999**.
[15] S. Iwata, C. Ostermeler, B. Ludwig, H. Michel, *Nature* **1995**, *376*, 660−669; T. Tsukihara, H. Aoyama, E. Yamashita, T. Tomizaki, H. Yamaguchi, K. Shinzawa-Itoh, R. Nakashima, R. Yaono, S. Yoshikawa, *Science* **1995**, *269*, 1069−1074.
[16] S. Brooker, V. McKee, *J. Chem. Soc., Dalton Trans.* **1990**, 2397−2401; J. McCrea, V. McKee, T. Metcalfe, S. S. Tandon, J. Wikaira, *Inorg. Chim. Acta* **2000**, *297*, 220−230.
[17] F. V. Lovecchio, E. S. Gore, D. H. Busch, *J. Am. Chem. Soc.* **1974**, *96*, 3109−3118; M. P. Suh, *Adv. Inorg. Chem.* **1997**, *44*, 93−146.
[18] S. Brooker, R. J. Kelly, *J. Chem. Soc., Dalton Trans.* **1996**, 2117−2122.
[19] G. J. Kubas, *Inorganic Syntheses, Vol. 28*, John Wiley and Sons, New York, **1990**, 68−70.
[20] S. Brooker, T. C. Davidson, S. J. Hay, R. J. Kelly, D. K. Kennepohl, P. G. Plieger, B. Moubaraki, K. S. Murray, E. Bill, E. Bothe, *Coord. Chem. Rev.* **2001**, *216−217*, 3−30.
[21] G. M. Sheldrick, *Acta Crystallogr., Sect. A* **1990**, *46*, 467−473; G. M. Sheldrick, *Methods Enzymol.* **1997**, *276*, 628−641.
[22] G. M. Sheldrick, T. R. Schneider, *Methods Enzymol.* **1997**, *277*, 319−343.
[23] P. van der Sluis, A. L. Spek, *Acta Crystallogr., Sect. A* **1990**, *46*, 194−201.

Received January 27, 2004
Early View Article
Published Online April 26, 2004

